國立交通大學
物理研究所
博士論文

量子光學中的表面電漿子問題

研 究 生：陳光胤
指導教授：江進福 褚德三

中華民國九十九年二月

量子光學中的表面電漿子問題

Quantum Optics with Surface Plasmons

研 究 生 : 陳光胤　　Student : Guang-Yin Chen

指導教授 : 江進福　　Adviser : Tsin-Fu Jiang

褚德三　　Der-San Chuu

國 立 交 通 大 學

物 理 研 究 所

博 士 論 文

A Thesis
Submitted to Institute of Physics
College of Science
National Chiao Tung University
in Partial Fulfillment of the Requirements
for the Degree of
Doctor of Philosophy
in

Physics

February 2010

Hsinchu, Taiwan

中華民國九十九年二月

量子光學中的表面電漿子問題

學生:陳光胤　　　　　　　　指導教授:江進福

褚德三

國立交通大學物理研究所

摘要

在本論文中，我們首先計算二能階單量子點激子耦合到量子線上的表面電漿子之衰變率，我們發現該衰變率因為其與表面電漿子的耦合非常強而被大大的提升。在色散曲線的相對極小值附近，衰變率甚至會被提昇至無窮大，這告訴我們在這一範圍內使用馬可夫近似是不恰當的，於是我們借用了在光子晶體中能隙附近的處理方式，以非馬可夫來重新計算量子點激子的衰變率之時間演化，並得到相對應的振盪行為。我們並提出藉由量子線上的表面電漿子的散射來達到雙量子點的糾纏態的想法，實際運算後發現，假使我們在量子線的兩端並沒有偵測到表面電漿子的訊號，這表示雙量子點的糾纏態已經產生。為了避免表面電漿子在傳播中耗散，我們提出使用兩個同時耦合到完美波導的小量子線來取代原有的長量子線，並介紹了 Lindblad 形式的

master 方程來涵蓋耗散的效應且進一步計算 concurrence 的時間演化。

Quantum Optics with Surface Plasmons

Student: Guang-Yin Chen **Adviser: Tsin-Fu Jiang**

Der-San Chuu

INSTITUTE OF PHYSICS
NATIONAL CHIAO TUNG UNIVERSITY

Abstract

In this thesis, we examine the spontaneous emission of a two-level emitter, quantum dot exciton, into surface plasmons propagating on the surface of a cylindrical nanowire. The numerically obtained dispersion relations are found to strongly influence the spontaneous emission rate. At certain values of the exciton bandgap, the emission rates can go to infinity due to the band-edge feature of the dispersion relations. Borrowing the idea from the photonic crystals, we model the quantum-dot exciton dynamics with a non-Markovian way and demonstrate that the decay can undergo an oscillatory behavior. In addition, we theoretically study coherent single surface-plasmon transport in a nanowire strongly coupled to two quantum dots. Using a real-space Hamiltonian we find analytical expressions for the transmission and reflection coefficients and dot-dot entanglement. Our results show that remotely entangled states can be created if there is no out-going surface plasmons detected at both ends of the wire. We further use two small wires evanescently coupled to a dielectric waveguide instead of a long wire to minimize the dissipations during propagation, and introduce the Lindblad form master equation to include the dissipations and calculate the concurrence dynamics.

誌謝

從碩一進入交大褚德三教授的實驗室的第一天開始，剛好五年半了，這段時間，是我人生至今最精采的時期，在各方面的成長也是最多，要感謝的人難以計數，也難以言表，但我仍想在此向一些人道謝：

謝謝我的父母和哥哥，謝謝你們一直以來的支持，讓我可以心無旁騖的專心在研究上，希望我是可以讓你們感到驕傲的。謝謝褚德三教授，謝謝您在臨退休之時，還願意收我入門，甚至在我碩班畢業時，也給我機會讓我繼續博士班的學業，多年以來從您的身上學到太多太多，除了物理之外，還有對這塊土地的愛護的心。謝謝成大物理系陳岳男教授，感恩你多年來帶領著我做研究，在各方面幫助我，讓我有機會四處出國訪問，讓我在學術的眼界及專業上，有長足的進步，我很珍惜這段亦師亦友的情誼，從你身上我看到了慈濟人的慈悲，這對我的個性和品格也有很大的助益。感謝江進福老師，感謝您願意在褚老師退休之後將我納入名下，我從您的課堂上學了很多，很佩服您一直以來在學術上的用功及專注。感謝交大電物系李仁吉教授，感謝您提供我許多教學的機會，讓我能一直成長，並對自己更有信心。感謝張正宏教授，謝謝您一直以來的照顧，並啟發了我去德國的念頭。感謝交大物理所林俊源所長、吳天鳴教授、孟心飛教授、林志忠教授、高文芳教授。謝謝你們多年來的照顧，我永遠不會忘記這個溫暖的地

方，永遠不會忘記這豐富的五年半碩博生涯。感謝成大物理系周忠憲教授，謝謝你在口試時提供的寶貴意見。

感謝我的好兄弟王瑞仁，謝謝你從碩士班開始一路的陪伴，我們的足跡遍佈整個台灣，難忘在低潮的時候，淡水河畔的互相打氣及你老是犧牲自己成全我的情義，這一切我都銘記在心，友誼長存！感謝交大物理所的夥伴們：蔡昆憲博士、劉宗哲、鄧德明、唐平翰、黃邦杰、葉永順、葛威成、張家銘、蔡政展，謝謝你們的多年陪伴，讓我在物理所非常的開心。感謝電物系薄膜物理實驗室的學長姊們：林高進博士，我很懷念我們一起從新竹開車回高雄，在車上天南地北的聊物理、人生；邱裕煌博士、李哲明博士、廖英彥教授、院繼組博士、周瑞雯博士、唐英瓚，我們一起努力過來的日子，我會永遠記得。感謝成大的學弟們：陳緯、陳宏斌，吳俊德、林瓚東、金功。

Here, I would like to give many thanks to my partners at university of Freiburg: Prof. Dr. Andreas Buchleitner, for taking good care of my stay in Germany. You are really a good mental tutor, scientist, and most important, a good friend. Dr. Florian Mintert, for supervising me and being good company. Dr. Fernando de Melo, for being such a good friend, you are really my man. Dr. Thomas Wellens, I really learned much form your Quantum Optics class. Dr. Markus Tiersh, you made me know more traditions, social situation, cultures about Germany. Torsten Scholak, for being a good partner in drinking and Japanese movies. Moritz, Viola, Max, Malte, Alexej, Felix E, Felix P, Stefan, Celsus, Tobias G, Tobias Z, Benno and Hannah, for treating me well. Dr. Joonwoo Bae at KIAS in Korea, thank you for being a good friend and always giving me good advice. Partners at Riken in Japan: Prof. Franco Nori, Dr. Neil Lambert, Dr. Koji Maruyama, I do enjoy each stay in Japan with you guys. 最後感謝國科會台德三明治計畫2008年秋季梯次的夥伴們，有你們的陪伴，德國這一年真是美好的經驗。

Contents

List of Figures

Chapter 1

Introduction

Surface plasmons, generated by collective vibrations of the local charge densities on the metallic surface, are propagating electromagnetic waves along the metal-dielectric interface (See Fig. 1.1). In 1957, Ritchie pioneeringly predicted the existence of the collective excitations of conduction electrons in a thin foil by calculating the energy losses of a fast electron passing through the thin foil [2]. In 1959, Powell an Swan experimentally showed the existence of the collective excitations [3], and the quanta of these excitations are first called "surface plasmons" in 1960 [4]. Since then, surface plasmons have been extensively studied both in theoretical and experimental investigations. Recently, the concept of plasmonics, in analogy to photonics, has received great attention since surface plasmons reveal strong analogies to light propagation in conventional dielectric components [5]. For examples, it

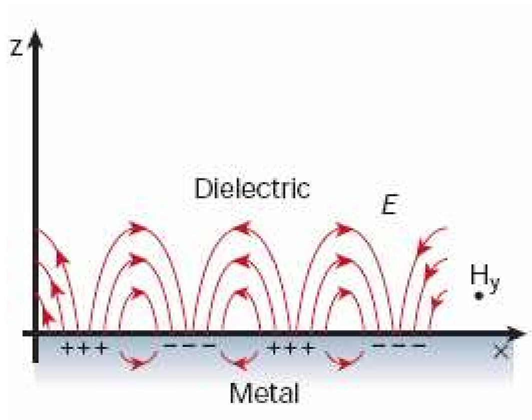

Figure 1.1: Schematic diagram of the surface plasmons [1].

is now possible to confine them to subwavelength scales [1] leading to novel approaches for waveguiding below the diffraction limit [6]. The combination of subwavelength confinement, single mode operation [7], and relatively low power propagation loss [8] of surface plasmon polaritons could be used to miniaturize existing photonic circuits [9], or implement plasmon-based computational logic in the THZ regime. In addition, high surface plasmon field confinement was also used to demonstrate an all-optical modulator [10].

Plasmon induced modification of the spontaneous emission (SE) is naturally an extended issue [11]. Sun *et al.* recently calculated the Lamb shift of a hydrogen atom due to the surface plasmon polariton [12]. Strong enhancement of fluorescence due to surface plasmons was also observed [13]. Coherent coupling between individual optical emitters and guided plasmon excitations in conducting nanowires at optical frequencies was also pointed out [14]. In chapter 2, we will therefore investigate the spontaneous emission (SE) rate of a quantum dot (QD) exciton into the surface plasmons in a metal nanowire. SE of a QD exciton into different modes of surface plasmons is considered separately. The emission rate is found to approach infinity at certain values of QD exciton bandgap, which is similar to the band-edge effect in photonic crystals. This enhancement has been experimentally observed by Akimov *et al.* [15] with an enhanced Purcell factor (Γ_{pl}/Γ'), which is about 2.5 at room temperature.

In 2007, D. E. Chang *et al.* proposed a novel approach [16] to form a "optical transistor" through the scattering of surface plasmons propagating on the surface of a metal wire. In a related context, advances in quantum information science (QIS) has promoted an experimental drive for physical realizations of highly entangled states [17]. Some success has been found within quantum-optical and atomic systems [18]. However, due to scalability requirements, solid-state realizations of such phenomena are the favored choices [19]. Furthermore, while initial success has been found by concentrating on coupling nearby qubits with local interactions [20], entangling arbitrary remote qubits is now an important goal. Circuit quantum electrodynamics (QED), for example, is one of the few promising candidates to couple two distant qubits via a cavity bus [21]. Motivated by these recent developments, we will in chapter 3 propose a scheme that can achieve the entanglement between two remote QD qubits coupled to the same metal wire.

To increase the efficiency of optical transmission, Pyayt *et al.* [22] proposed that the nanowires lay perpendicular to the polymer waveguide with one end inside the polymer. They theoretically predicted and experimentally demonstrated the control over the degree of coupling by changing the light polarization. Furthermore, B. Dayan *et al.* [23] proposed a "photon turnstile" to demonstrate an efficient mechanism for the regulated transport of photons one by one by using a microscopic optical resonator evanescently coupled to a fiber. From these, we propose to use two small wires evanescently coupled to a dielectric wave guide instead of using a long wire to increase the transmission efficiency of the surface plasmons in chapter 4. This also enables us to minimize the Ohmic losses during propagation.

More recently, surface plasmon is discovered to be a new dimension to store information [24]. And the basic quantum mechanical property for a quantum particle, that is the duality of surface plasmons, has been also examined [25]. Moreover, in stead of using the conventional far-field optical detection, Falk *et al.* [26] proposed a new all-electrical surface plasmon polaritons detection techniques based on the near-field coupling between guided plasmons and a nanowire field-effect transistor to detect the plasmon emission from an individual colloidal quantum dot coupled to a surface plasmon polaritons waveguide. In this way, one could not only preserve the better efficiency and miniaturization of photonic circuits but also have the advantage of electrically near-field detection.

In the last chapter, we will summarize this thesis and propose a future work on the simulation of quantum phase transition [27, 28] by considering one QD coupled to a small nanowire as a site of a one-dimensional array. Bose-Hubbard model can then be simulated if each site is coupled to its nearest neighbors.

Chapter 2

Spontaneous emission of excitons into surface plasmons

2.1 Dispersion relations of surface plasmons

Consider now a colloidal CdSe/ZnS quantum dot (QD) near a cylindrical silver nanowire with radius a. The QD and nanowire are assumed to be separated by a GaN layer [29] as shown in Fig. 2.1. One of the main reasons to choose a CdSe/ZnS QD exciton as the two-level emitter is that it is now possible to isolate single colloidal QD and measure its exciton lifetime [30]. The other reason is that its exciton bandgap is around $2eV$ to $2.5eV$, depending on the size and environment of the dot [31]. The plasmon energy $\hbar\omega_p$ of bulk silver is 3.76 eV with the corresponding saturation energy

$\hbar\omega_p/\sqrt{2} \approx 2.66eV$ in the dispersion relation [32]. As we shall see below, variations of the dispersion relations in energy just match the exciton bandgap of colloidal CdSe/ZnS QDs.

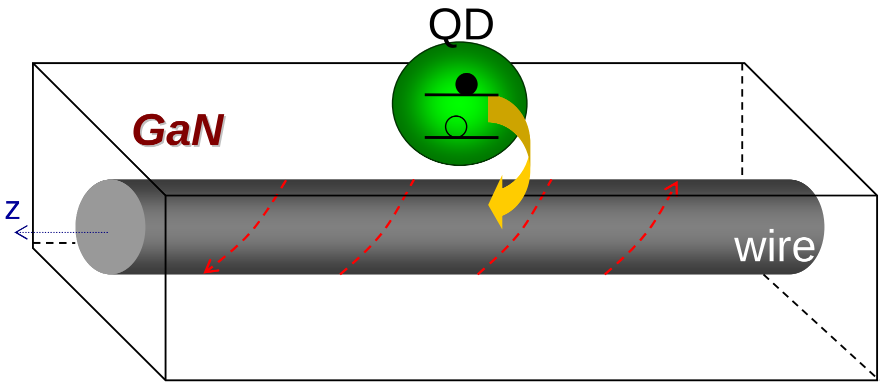

Figure 2.1: Schematic view of the model: Spontaneous emission of a two-level emitter (QD exciton) into nanowire surface plasmons, which act like photons in a cavity.

Surface plasmon modes are created due to the nonzero local charge density on the surface of a nanowire. The n-th surface plasmon mode's components of the electromagnetic field at the surface can be obtained by solving Maxwell's equations in a cylindrical geometry (ρ and φ denote the radial and azimuthal coordinates, respectively) with the appropriate boundary conditions [33]:

$$
\begin{aligned}
E_\rho &= [\frac{ik_z}{K_\xi}\frac{d\psi_n^\xi(K_\xi\rho)}{d(K_\xi\rho)}A_n^\xi - \frac{\mu_\xi\omega n}{K_\xi^2\rho}\psi_n^\xi(K_\xi\rho)B_n^\xi]\phi_n,\\
E_\varphi &= -[\frac{nk_z}{K_\xi^2\rho}\psi_n^\xi(K_\xi\rho)A_n^\xi - \frac{i\mu_\xi\omega}{K_\xi}\frac{d\psi_n^\xi(K_\xi\rho)}{d(K_\xi\rho)}B_n^\xi]\phi_n,\\
E_z &= [\psi_n^\xi(K_\xi\rho)A_n^\xi]\phi_n,\\
H_\rho &= [\frac{n(K_\xi^2+k_z^2)}{\mu_\xi\omega K_\xi^2\rho}\psi_n^\xi(K_\xi\rho)A_n^\xi + \frac{ik_z}{K_\xi}\frac{d\psi_n^\xi(K_\xi\rho)}{d(K_\xi\rho)}B_n^\xi]\phi_n,\\
H_\varphi &= [\frac{i(K_\xi^2+k_z^2)}{\mu_\xi\omega K_\xi}\frac{d\psi_n^\xi(K_\xi\rho)}{d(K_\xi\rho)}A_n^\xi - \frac{nk_z}{K_\xi^2\rho}\psi_n^\xi(K_\xi\rho)B_n^\xi]\phi_n,\\
H_z &= [\psi_n^\xi(K_\xi\rho)B_n^\xi]\phi_n, \qquad (2.1)
\end{aligned}
$$

with

$$
\begin{aligned}
&K_\xi^2 = \omega^2\epsilon_\xi(\omega)/c^2 - k_z^2 \ \ (\xi = I \text{ or } O),\\
&\psi_n^I(K_I\rho) = J_n(K_I\rho),\ \psi_n^O(K_O r) = H_n^{(1)}(K_O\rho),\\
&\phi_n = exp(in\varphi + ik_z z - i\omega t),
\end{aligned}
$$

where $J_n(K_I\rho)$ and $H_n^{(1)}(K_O\rho)$ are Bessel and Hankel functions, respectively. I (O) stands for the component inside (outside) the wire. The dielectric function is assumed as $\epsilon(\omega) = \varepsilon_\infty[1 - \frac{\omega_p^2}{\omega(\omega+i/\tau)}]$, where $\epsilon_\infty = 9.6$ (for Ag) and $\epsilon_\infty = 5.3$ (for GaN). The plasma energy $(\hbar\omega_p)$ of bulk silver is 3.76 eV, and $\tau = 3.1\times10^{-14}$ s is the relaxation time due to ohmic metal loss [34], which has been taken into account in the following calculations. The magnetic permeabilities $\mu_{I,O}$ are unity everywhere since we consider nonmagnetic materials here. A_n^ξ and B_n^ξ are constants to be determined by normalizing the electromagnetic field to the vacuum fluctuation energy, $\int \epsilon(|E_\rho|^2 + |E_\varphi|^2 + |E_z|^2) d\mathbf{r} = \hbar\omega(\mathbf{k})$, and matching the boundary conditions. According to the experiment [35], the length of a nanowire is very long comparing to the size of the QD. Therefore, it's legitimate to treat the length of the nanowire as effectively infinite. In this case, the dispersion relations of the surface plasmons with a continuum spectrum can be obtained by solving the following transcendental equation numerically [33]:

$$
\begin{aligned}
& S(k_z, \omega) = \\
& [\frac{\mu_I}{K_I a}\frac{J_n'(K_I a)}{J_n(K_I a)} - \frac{\mu_O}{K_O a}\frac{H_n^{(1)\prime}(K_O a)}{H_n^{(1)}(K_O a)}][\frac{(\omega/c)^2\varepsilon_I(\omega)}{\mu_I K_I a}\frac{J_n'(K_I a)}{J_n(K_I a)} \\
& - \frac{(\omega/c)^2\varepsilon_O(\omega)}{\mu_O K_O a}\frac{H_n^{(1)\prime}(K_O a)}{H_n^{(1)}(K_O a)}] - n^2 k_z^2 [\frac{1}{(K_O a)^2} - \frac{1}{(K_I a)^2}]^2 \\
& = 0.
\end{aligned} \tag{2.2}
$$

Fig. 2.2(a) shows the dispersion relations of the $n = 0$ mode for different radii. Here, one unit of the effective radii R ($\equiv \omega_p a/c$) is roughly equal to 53.8 nm. As can be seen, the behavior of these curves is very similar to the two-dimensional case [17], i.e. $\Omega(\equiv \omega/\omega_p)$ gradually saturates with increasing wave vector $K(\equiv k_z c/\omega_p)$. This is because the fields for the $n = 0$ mode are

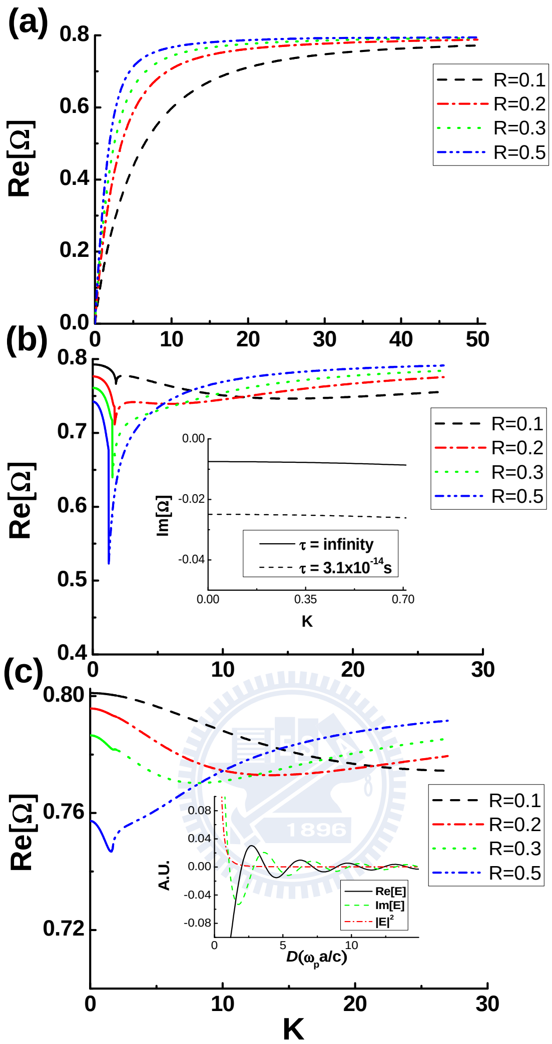

Figure 2.2: (a), (b), and (c) represent the dispersion relations of surface plasmons for the modes $n = 0$, 1, and 2, respectively. The non-solid (solid) lines represent the bound (non-bound) modes. The units for vertical and horizontal lines are $\Omega = \omega/\omega_p$ and $K = k_z c/\omega_p$, and $R \equiv \omega_p a/c$. The inset in (c) represents the real part, imaginary part, and intensity of the electric field for $n = 1$ non-bounded mode as a function of distance away from the wire surface.

independent of the azimuthal angle φ. However, the behaviors for the $n \neq 0$ modes are quite different as shown in Fig. 2.2(b) and (c). The first interesting point is the discontinuities around $\omega/c \approx k_z$. Further analysis shows that the solutions of ω are "almost real" [36] as $k_z > Re[\omega]/c$. In this case, the first kind Hankel function of order n, $H_n^{(1)}(K_\xi \rho)$, decays exponentially. This means the surface plasmons in this regime are confined on the surface (*bound modes*). For $k_z < Re[\omega]/c$, however, the solutions of ω are *complex*. The form of $H_n^{(1)}(K_\xi \rho)$ in this case is like a traveling wave (*non-bound modes*), for which its lifetime is finite. One might think that the reason for the finite lifetime is totally from the ohmic metal loss. However, as shown in the inset of Fig. 2.2(b), the frequency is still complex (the solid line) even without the metal loss τ. We thus conclude that the finite lifetime in the regime of k_z $< Re[\omega]/c$ is actually influenced by both metal and radiation loss.

2.2 Rate enhancement due to band-edge effect

To calculate the SE rate of a QD or atom within a structured reservoir, one in general considers the contributions from the scattered fields for different surface geometry of surrounding scatters. There are some well-developed methods to deal with such calculations. For instance, making use of the Green's tensors, one can calculate the scattered fields and obtain the local density of states for an atomic dipole [37]. Once the surfaces of scatters are metallic, the presence of surface plasmons are expected to dominate the SE rate due to the strong coupling between surface plasmons and QD [14]. A simple explanation why the coupling is so strong is that the density of energy stored in the electric fields of surface-plasmon modes must be equal to half the vacuum fluctuation energy, $\frac{1}{2}\int \epsilon(|E_\rho|^2+|E_\varphi|^2+|E_z|^2)d\mathbf{r} = \frac{1}{2}\hbar\omega(\mathbf{k})$. Since the volume of the wire is very small, the electric field is supposed to be very strong. In our case, we would like to focus on the decay into surface plasmons on the SE rate, since other contributions of the scattering fields are much smaller than that of the surface plasmons.

The general decay rate of a QD or atom coupled to multi-mode electromagnetic fields can be directly obtained from Fermi's golden rule [38] within the dipole approximation:

$$\Gamma_{sp} = \frac{2\pi}{\hbar}\int d\vec{k}\ |\vec{d}_0 \cdot \vec{E}(\vec{k})|^2 \delta(\omega_{eg} - \omega_{\vec{k}}), \tag{2.3}$$

where $\omega_{\vec{k}}$ and $\vec{k}$ are the frequency and wave vector of the field $\vec{E}(\vec{k})$, respectively. $\vec{d}_0$ is the dipole moment of the QD exciton, and ω_{eg} is the exciton bandgap of the QD. Once the electromagnetic fields are determined, the SE rate, Γ_{sp}, of the QD excitons into bound surface plasmons can be obtained via Eq. (2.3). Since the surface plasmons are confined on the surface [39] of the cylindrical nanowire, the integral of $\vec{k}$ in Eq. (2.3) stands for the summation of the contributions from all possible final states, i.e. a two-dimensional integral of k_φ and k_z. Because n is the quantum number governing the φ-component of the wavefunction, summing over all n-mode is equivalent to integrate over all k_φ. For convenience, we assume the dipole moment $\vec{d}_0$ is along the ρ-direction. By transforming the argument of the delta function from $\omega_{\vec{k}}(=\omega_{n,k_z})$ to k_z as

$$\delta(\omega_{eg}-\omega_{\vec{k}})=\sum_{k_{z_i}}\frac{1}{|\frac{d(\omega_{eg}-\omega_{n,k_z})}{dk_z}|_{k_{z_i}}}\delta(k_z-k_{z_i}),$$

the SE rate can then be written as

$$\Gamma_{sp}=\sum_{n=0}^{\infty}\Gamma_n=\frac{2\pi}{\hbar}\sum_{n=0}^{\infty}\frac{\sum_{k_{z_i}}|\vec{d}_0\cdot\vec{E}_\rho(k_{z_i})|^2}{|\frac{d(\omega_{eg}-\omega_{n,k_z})}{dk_z}|_{k_{z_i}}}, \tag{2.4}$$

where Γ_n is the SE rate into the n-th mode, and k_{z_i} stands for the values of k_z that make the argument in the δ function vanish. For the purpose of discussion, we display the SE rate into the first few modes (Γ_n, $n=0,1,2,3$) as shown in Fig. 2.3 and 2.4 for $R=0.1$ and 0.5, respectively. In plotting Fig. 2.3 and 2.4, the distance between the dot and the wire surface is fixed as $\ell=10.76\ nm$. We find that the latter modes ($n>3$) contribute much less to the decay rate. For certain ranges of ω_{eg}, the contributions to the decay rate Γ_{sp} mainly come from the first few modes. For example, if we set $\omega_{eg}=0.74647$, which is the minimum point of the

$n = 1$ mode dispersion curve, the decay rate (for $R = 0.1$ case) is mainly from $n = 0$ and $n = 1$ modes as seen from Fig. 2.3. In addition, the novel feature here is that the SE rate approaches infinity at certain values of the exciton bandgap ω_{eg}. Mathematically, one might think that at these values the corresponding slopes of the dispersion relation are zero [40]. Physically, however, this infinite rate is not reasonable since it's based on perturbation theory. Therefore, one has to treat the dynamics of the exciton around these values more carefully, i.e. the *Markovian* SE rate is not enough. One has to consider the *non-Markovian* behavior around the band-edge, which means the band abruptly appears/disappears across certain values of ω_{n,k_z}.

2.3 Non-Markovian dynamics of QD excitons

When a open quantum system interacts with a structured reservoir, there exists non-Markovian memory effect in the form of oscillatory behavior of decay dynamics which reflects the exchanges of information back and forth between system and reservoir. Recently, J. Piilo *et al* developed a non-Markovian Quantum Jumps method [41] which generalized the proved Monte Carlo wave function method for the Markovian system in order to deal with the non-Markovian problems. Here, we will numerically solve the time-dependent Schrödinger equation to obtain the time-dependent population on the excited state.

To obtain the non-Markovian dynamics of the exciton, we first write down the Hamiltonian of the system in the interaction picture (with the rotating wave approximation),

$$\begin{aligned} H_{ex-sp} &= \sum_{n,k_z} \hbar\Delta_{n,k_z}\widehat{a}^{\dagger}_{n,k_z}\widehat{a}_{n,k_z} \\ &\quad +\hbar\sum_{n,k_z}(g_{n,k_z}\sigma_{ge}\widehat{a}^{\dagger}_{n,k_z} + g^{*}_{n,k_z}\sigma_{eg}\widehat{a}_{n,k_z}), \end{aligned} \tag{2.5}$$

where $\sigma_{ij} = |i\rangle\langle j|(i,j = e,g)$ are the atomic operators; $\widehat{a}_{n,k_z}$ and $\widehat{a}^{\dagger}_{n,k_z}$ are the radiation field (surface plasmon) annihilation and creation operators; $\Delta_{n,k_z} = \omega_{n,k_z} - \omega_{eg}$ is the detuning of the radiation mode frequency ω_{n,k_z} from the excitonic resonant frequency ω_{eg}, and $g_{n,k_z} = \vec{d}_0 \cdot \overrightarrow{E}_{n,k_z}$ is the atomic field coupling.

Assuming there is an exciton in the dot with no plasmon excitation in the wire initially, the wavefunction of the system then has the form

$$|\psi(t)\rangle = b_e(t)\,|e,0\rangle + \sum_{n,k_z} b_{n,k_z}(t)\,|g,1_{n,k_z}\rangle\, e^{-i\Delta_{n,k_z}t}. \tag{2.6}$$

The state vector $|e,0\rangle$ describes an exciton in the dot and no plasmons present, whereas $|g,1_{n,k_z}\rangle$ describes the exciton recombination and a surface plasmon emitted into mode k_z. With the time-dependent Schrödinger equation, the solution of the coefficient $b_e(t)$ in z-space is straightforwardly given by

$$\widetilde{b}_e(z) = [z + \sum_{n=0}^{\infty} \int g_{n,k_z} g^*_{n,k_z} \frac{dk_z}{z + i(\omega_{n,k_z} - \omega_{eg})}]^{-1}. \tag{2.7}$$

We use the dispersion relations obtained from Eq. (2.2) to numerically calculate the integral over the whole spectrums of n and k_z in Eq. (2.7). Consequently, $b_e(t)$ can be obtained by performing a numerical inverse Laplace Transformation to Eq. (2.7).

The dashed, dotted, and dash-dotted lines in Fig. 2.5(a) represent the decay dynamics of the QD excitons for different detunings: $\delta = -0.4\gamma_0$, $0.4\gamma_0$, and $0.8\gamma_0$, respectively. Here, $\delta = \omega_0 - \omega_{n=1,k_z}$ is the detuning from the local minimum of the $n = 1$ mode, and γ_0 is the decay rate of the QD exciton into free space. The radius of the wire and the wire-dot separation are $R = 0.1$ and $\ell = 0.34$, respectively. Apparently, there exists oscillatory behavior in the decay profile, demonstrating that decay dynamics is non-Markovian. If one considers only the contribution from the $n = 1$ mode and set the detuning $\delta = 0$, the probability amplitude would saturate to a steady limit as shown by the solid line. This *quasi-dressed* state is an analogy of Rabi-oscillation in cavity quantum electrodynamics, and also appears in the systems of photonic crystals [42]. In the investigations for SE of a two-level atom near the edge of a photonic band gap, the density of states becomes singular, and the dispersion relation near the band edge can be approximated as a parabolic curve [42]. The oscillatory behavior during the decay can be then obtained by treating the transition from the excited state to the intermediate state as the other decay channel. The oscillatory behavior in the photonic crystal case is a direct consequence of strong interaction between the atom and its own localized radiation. In our case, the coupling between the QD exciton and surface plasmons can be very strong as well, resulting from a similar feature of local extremum in the dispersion curve. So, the oscillations in decay dynamics shown in Fig. 2.5(a) can be understood as the SE near a band-edge.

Another interesting discovery is shown in Fig. 2.5(b) if one sets the detuning $\delta = 0$ and plots the dynamics of the exciton for different dot-wire separations: $\ell = 0.2$ (dotted line), $\ell = 0.3$ (solid line), and $\ell = 0.35$ (dashed line). As can be seen, the oscillatory behavior is diminished when decreasing the dot-wire separation. This is because, as ω_{eg} is chosen to be close to the local minimum of the dispersion relation of the $n = 1$ mode, the decay dynamics is mainly dominated by the contributions from $n = 0$ and $n = 1$ modes. Since the non-Markovian oscillatory behavior is mainly from the local minimum of $n = 1$ mode, the contribution from the $n = 1$ mode can be overwhelmed by that from the $n = 0$ mode if the dot is put close enough to the wire surface. This leads to a degradation of the oscillatory behavior.

2.4 Conclusion

In this chapter, we have numerically calculated the dispersion relations of nanowire surface plasmons propagating on the surface of a silver nanowire and have shown that SE of QD excitons into surface plasmons can be greatly enhanced at certain values of the exciton bandgap. The enhancement is due to the strong coupling between QDs and the surface plasmons, and also the band-edge effect [28] in dispersion relation. A non-Markovian way has been used to treat the unreasonable infinitely-enhanced SE rate around the band edge. With this treatment, we observe the oscillatory decay dynamics of QD excitons. This band-edge effect can be analogous to the case that when a two-level atom near the edge of photonic band gap: the density of state is singular and the dispersion curves can be approximated as a parabolic curve coinciding with the local minimum point in our dispersion relations for $n \geq 1$ modes.

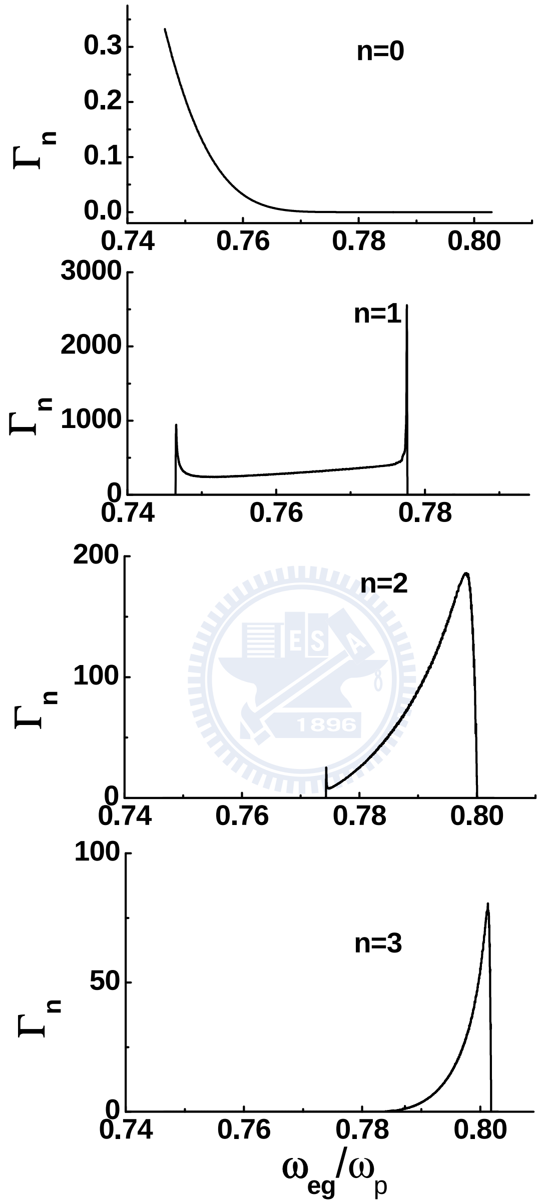

Figure 2.3: Spontaneous emission rate (Γ_n) into $n = 0 \sim 3$ modes for $R = 0.1$. The unit of Γ_n is normalized to free space decay rate γ_0.

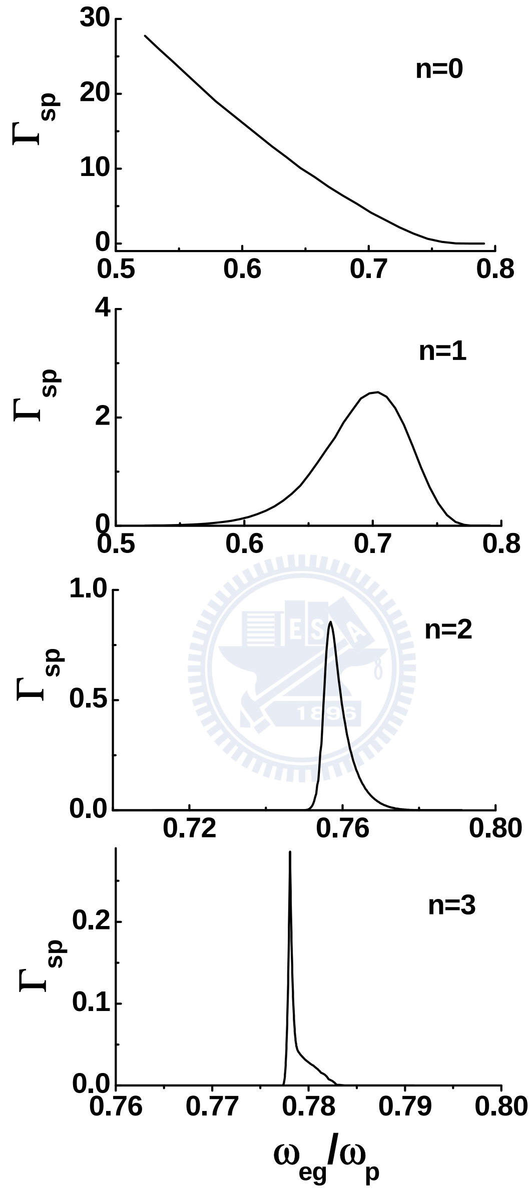

Figure 2.4: Spontaneous emission rate (Γ_n) into $n = 0 \sim 3$ modes for $R = 0.5$. The unit of Γ_n is normalized to free space decay rate γ_0.

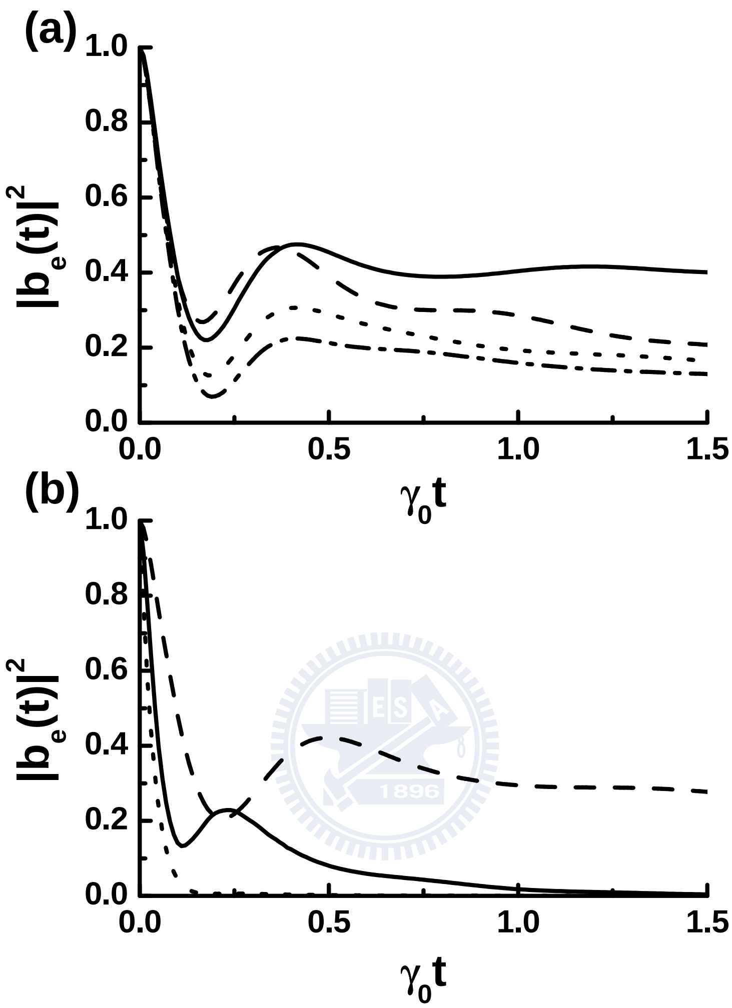

Figure 2.5: (a) Non-Markovian decay dynamics of QD excitons for $\delta = -0.4\gamma_0$ (dashed line), $0.4\gamma_0$ (dotted line), and $0.8\gamma_0$ (dash-doted line). As $\delta = 0$, the solid line represents the result for the contribution from $n = 1$ mode. (b) By setting $\delta = 0$, the dotted, solid, and dashed lines represent the results for dot-wire separation $d = 0.2$, 0.3, and 0.35, respectively. Here, one unit of d is $\omega_p a/c = 53.8\ nm$.

Chapter 3

Coherent single surface plasmon transport

3.1 Scattering of surface plasmons

We propose in this chapter a novel scheme that can entangle two remote QD qubits coupled to a metal nanowire. The idea is inspired by recent experiments showing single surface plasmons in metallic nanowires coupled to QDs [15]. We will use a real-space Hamiltonian to treat the coherent surface-plasmon transport in the wire coupled to two dots. It will be found maximally entangled states can be created if the separation between the two dots is equal to multiple half-wavelength of the optical plasmon. Furthermore, we will show the entangled state can also be stored in the metastable states,

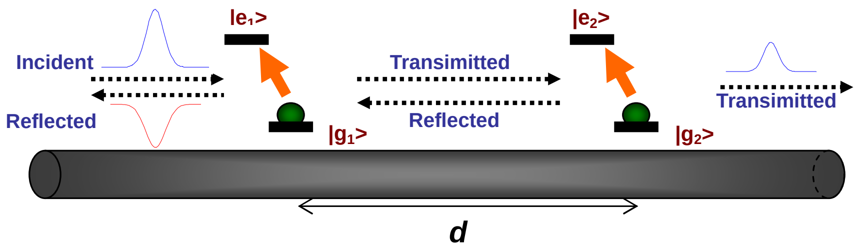

Figure 3.1: Schematic view of a metal nano-wire coupled with two QDs. A single surface plasmon injected from the left is coherently scattered by the dots.

which are decoupled from the surface plasmons, by applying classical laser pulses to each QD separately. The storage efficiency of the entangled states is equal to $1 - 1/P$, where P is the Purcell factor of the QD excitons.

When a semiconductor QD is put close to a metal nanowire, strong coupling between the QD exciton and surface plasmons can occur [14], as in traditional cavity QED. In the following, we consider two QDs, separated by a distance of d, near a cylindrical metal nanowire with radius a as shown in Fig. 3.1. The Hamiltonian of the two-level QDs (with energy spacing $\hbar\omega_{eg}$) and the surface plasmons can be written as [16]

$$
\begin{aligned}
H = &\sum_{j=1,2} \hbar[\omega_{eg} - i(\frac{\gamma_0 + \Gamma_0}{2})]\sigma_{e_j,e_j} \\
&- i\hbar\frac{sin(k_0 d)}{2k_0 d}\gamma_0(\sigma_{e_1,e_2} + \sigma_{e_2,e_1}) \\
&- \hbar g \int dk\ [(\sigma_{e_1,g_1} + \sigma_{e_2,g_2}e^{ikd})a_k + h.c.] \\
&+ \int dk\ \hbar v_g |k| a_k^{\dagger} a_k,
\end{aligned}
\tag{3.1}
$$

where $\sigma_{e_j,e_j}(\sigma_{e_j,g_j})= |e_j\rangle\langle e_j|(|e_j\rangle\langle g_j|)$ represents the diagonal (off-diagonal) element of the j-th QD operator, and $a_k^{\dagger}$ is the creation operator of the surface plasmon. Here, γ_0 and Γ_0 denote the decay rates into free space and other non-radiative channels, respectively. v_g is the velocity of the surface plasmon, $k_0 = \omega_{eg}/v_g$, and g is the coupling constant between the excitons and surface plasmons. The third term in the first line of Eq. (3.1) represents the effect of collective decay (super-radiance) [44]. Transforming Eq. (3.1) into real space, one obtains

$$
\begin{aligned}
H = &\hbar \int dx\{-iv_g c_R^{\dagger}(x)\frac{\partial}{\partial x}c_R(x) + iv_g c_L^{\dagger}(x)\frac{\partial}{\partial x}c_L(x) \\
&+ \hbar g \sum_{j=1,2} \delta(x-(j-1)d)[c_R^{\dagger}(x)\sigma_{g_j,e_j} + c_R(x)\sigma_{e_j,g_j} \\
&+ c_L^{\dagger}(x)\sigma_{g_j,e_j} + c_L(x)\sigma_{e_j,g_j}]\} \\
&+ \sum_{j=1,2}[E_e - i\hbar(\frac{\gamma_0 + \Gamma_0}{2})]\sigma_{e_j,e_j} \\
&- i\hbar\frac{sin(k_0 d)}{2k_0 d}\gamma_0(\sigma_{e_1,e_2} + \sigma_{e_2,e_1}) + E_g\sigma_{g_j,g_j},
\end{aligned}
\tag{3.2}
$$

where $E_e - E_g = \hbar\omega_{eg}$ and $c^{\dagger}_R(x)$ $[c^{\dagger}_L(x)]$ is a bosonic operator creating a right-going (left-going) photon at x. Assuming that a photon is coming from the left with energy $E_k = v_g k$. The stationary state of the system is written as

$$\begin{aligned} |E_k\rangle \;&=\; \int dx[\phi^{\dagger}_{k,R}(x)c^{\dagger}_R(x) + \phi^{\dagger}_{k,L}(x)c^{\dagger}_L(x)]|g_1, g_2, 0\rangle \\ &\quad + \sum_{j=1,2} e_{k_j}\sigma_{e_j,g_j}|g_1, g_2, 0\rangle, \end{aligned} \tag{3.3}$$

where $|g_1, g_2, 0\rangle$ means that both QD-1 and -2 are in the ground state with zero photon and e_{k_j} is the probability amplitude of the j-th QD in the excited state. For a photon incident from the left, $\phi^{\dagger}_{k,R}(x)$ and $\phi^{\dagger}_{k,L}(x)$ takes the form

$$\begin{cases} \phi^{\dagger}_{k,R}(x) \equiv exp(ikx)[\theta(-x) + a\ \theta(x)\theta(d-x) + t\ \theta(x-d)], \\ \phi^{\dagger}_{k,L}(x) \equiv exp(-ikx)[r\ \theta(-x) + b\ \theta(x)\theta(d-x)], \end{cases} \tag{3.4}$$

where t and r are the transmission and reflection amplitudes, respectively. $a\ exp(ikx)\theta(x)\theta(d-x)$ and $b\ exp(-ikx)\theta(x)\theta(d-x)$ represent the wave-function of the photon between 0 and d. From the eigenvalue equation $H|E_k\rangle = E_k|E_k\rangle$, we obtain the following relations for the coefficients

$$\begin{cases} g(2ae^{ikd} + 2be^{-ikd}) - \frac{i}{2}\frac{sin(k_0 d)}{kd}\gamma_0 e_{k_1} = (E_k/\hbar - \omega_{eg})e_{k_2}, \\ g(1 + a + r + b) - \frac{i}{2}\frac{sin(k_0 d)}{k_0 d}\gamma_0 e_{k_2} = (E_k/\hbar - \omega_{eg})e_{k_1}, \\ ge_{k_1} = iv_g(a-1),\ a = r - b + 1, \\ ge_{k_2} = iv_g(t-a)e^{ikd},\ \text{and } t = a +\ be^{-2ikd}. \end{cases} \tag{3.5}$$

The transmission and reflection amplitudes can then be determined algebraically.

Fig. 3.2(a) numerically displays the transmission coefficients $|t|^2$ (dashed lines) and reflection coefficients $|r|^2$ (solid lines) for different inter-dot distance. It is evident that the peak positions of the reflection coefficients deviate from the center ($\delta = 0$). The inset in Fig. 3.2(a) shows the peak positions as a function of kd. The green (blue) line represents the result with (without) super-radiant effect. As can be seen, not only the interference from the inter-dot separation, but also the super-radiance affects the positions of the peaks. Fig. 3.2(b) shows that the amplitude of reflection coefficients is suppressed when increasing metal loss Γ_0. Another interesting point is that the reflection coefficients have minimum points in the regime of $\delta < 0$. In the limit of large d, the super-radiant effect can be neglected. By setting $\Gamma' = \gamma_0 + \Gamma_0$, the positions of the minimum points, $\delta_{\min}$, can be deduced from Eq. (3.5) and satisfy the following relation:

$$-\tan^2(kd) = -4(\frac{\delta_{\min}}{\Gamma_{pl}})^2 - (\frac{\Gamma'}{\Gamma_{pl}})^2. \tag{3.6}$$

If there is no reflection ($r = 0$), one can say that Eq. (3.6) is the resonant tunneling condition for a photon travelling through two QDs, as an electron tunnel through a barrier.

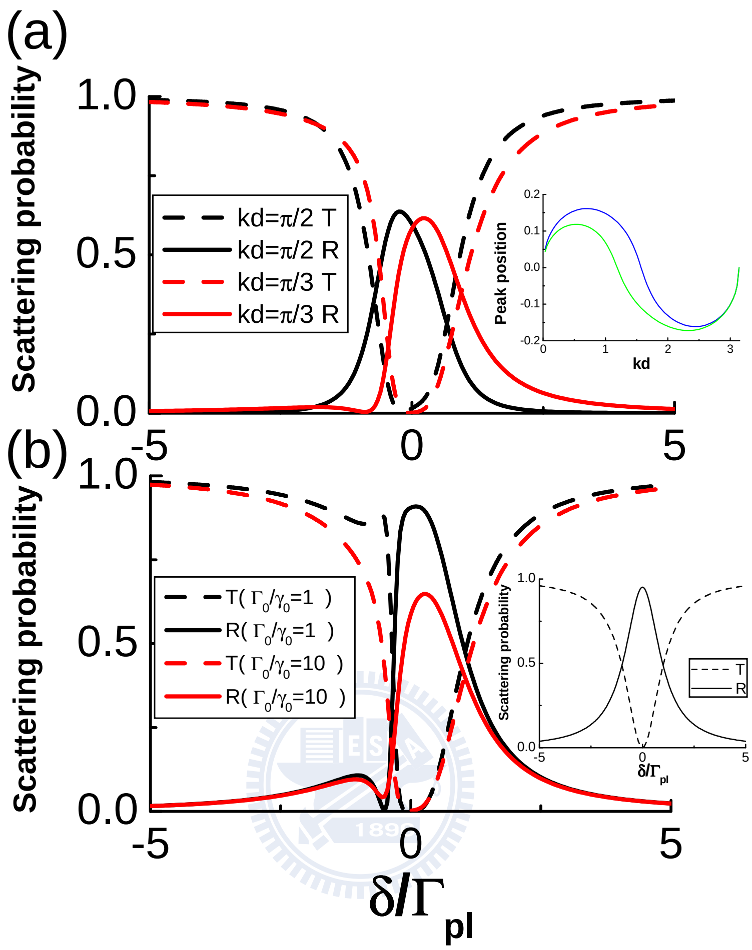

Figure 3.2: Transmission probabilities $|t|^2$ (dashed lines) and reflection probabilities $|r|^2$(solid lines) for a single surface plasmon incident on two QDs, as a function of detuning δ. In plotting the figures, we have assumed that $\gamma_0 = \Gamma_0 = 0.025\Gamma_{pl}$ in (a), and $kd = \pi/4$ in (b). The inset in (a) shows the peak positions of the reflection probabilities as a function of kd. The green (blue) line represents the result with (without) super-radiant effect. The inset in (b) is the result of a surface plasmon incident on a single dot [16].

3.2 Entanglement creation and storage

Eq. (3.3) and Eq. (3.5) also tell us that if there is no transmission or reflection photon detected at the two ends of the wire, the wavefunction collapses into the state: $\sum_{j=1,2} e_{k_j}\sigma_{e_j,g_j}|g_1, g_2, 0\rangle$. This means that it is possible to create entanglement between the two dots. Two special cases are that if $kd = 2n\pi$ or $(2n+1)\pi$ with n being an integer, the amplitude e_{k1} is equal to e_{k2} or $-e_{k2}$, respectively. In this case, the two-dot qubits become triplet or singlet entangled if no photon is detected. Fig. 3.3(a) shows the concurrence C of the two-dot qubits as functions of inter-dot distance and detuning δ. In addition to the special cases mentioned above, there is another oblique line satisfying the condition of maximum entanglement ($C = 1$). In the limit of large d, we find that the equation of this line is give by

$$\delta = -(\Gamma_{pl} + \Gamma')\tan(kd). \tag{3.7}$$

The physical meaning is that even the energy of the incident photon is not resonant with the qubit energy $\hbar\omega_{eg}$, it is still possible to achieve the maximum entangled states, only if the two dots are put at the right positions. The price to pay is that the entangled state now becomes $e_{k_1}|e_1, g_2\rangle + e^{i\theta}\cdot e_{k_2}|g_1, e_2\rangle$, i.e. there is an extra phase θ between $|e_1, g_2\rangle$ and $|g_1, e_2\rangle$. Fig. 3.3(b) shows the variations of the phase θ as a function of detuning δ. In the limit of $\gamma_0 \to 0$, black, red, and blue lines represent the results of $\Gamma_0 = 0$, 0.025, and $0.125\Gamma_{pl}$, respectively. As can be seen, once the metal loss, Γ_0, appears, the phase instantaneously changes from π(black line) to 0(red and blue lines) at the point $\delta = 0$. In Fig. 3.4, we show the density plot of the Concurrence versus kd and δ. The two different cases of maximal entanglement can be clearly seen.

One might argue that the created entangled states are irrelevant since the QDs are still coupled to the surface plasmons. The entanglement would eventually disappear due to radiative or non-radiative loss. To overcome this, one can consider multilevel emitters, such as the three-level configuration shown in Fig. 3.5. Metastable states, $|s_1\rangle$ and $|s_2\rangle$, are decoupled from the surface plasmons, but are resonantly coupled to $|e_1\rangle$ and $|e_2\rangle$, respectively, via a classical optical control field with Rabi frequencies $\Omega_1(t)$ and $\Omega_2(t)$.

Instead of transforming Eq. (3.1) into real space, the Hamiltonian is now represented under the bases of singlet, $|S\rangle = \frac{1}{\sqrt{2}}(|e_1, g_2\rangle - |g_1, e_2\rangle)$, and triplet, $|T\rangle = \frac{1}{\sqrt{2}}(|e_1, g_2\rangle + |g_1, e_2\rangle$, states:

$$\begin{aligned} H &= \hbar(\omega_{eg} - i\frac{\Gamma'}{2})(|T\rangle\langle T| + |S\rangle\langle S|) \\ &\quad -\hbar g \int dk \ \{[\frac{1}{\sqrt{2}}(1 + e^{ikd})\,|T\rangle\langle g_1, g_2|\, a_k \\ &\quad +\frac{1}{\sqrt{2}}(1 - e^{ikd})\,|S\rangle\langle g_1, g_2|\, a_k] + h.c.\} \\ &\quad +\int dk \ \hbar v_g |k| a_k^\dagger a_k, \end{aligned} \tag{3.8}$$

where $\Gamma' = \gamma_0 + \Gamma_0$ again is from the approximation that super-radiant effect can be neglected in the limit of large d. We now consider the general time-dependent wave function

$$
\begin{aligned}
|\psi\rangle &= \int dk[c_{R,k}(t)\hat{a}^{\dagger}_{R,k} + c_{L,-k}(t)\hat{a}^{\dagger}_{L,-k}]\,|g_1, g_2; vac\rangle \\
&+c_T(t)\,|T; vac\rangle + c_S(t)\,|S; vac\rangle \qquad (3.9)\\
&+c_{M_T}(t)\,|M_T; vac\rangle + c_{M_S}(t)\,|M_S; vac\rangle\,,
\end{aligned}
$$

where $|M_S\rangle[= \frac{1}{\sqrt{2}}(|s_1, g_2\rangle - |g_1, s_2\rangle)]$ and $|M_T\rangle[= \frac{1}{\sqrt{2}}(|s_1, g_2\rangle + |g_1, s_2\rangle)]$ denote the singlet and triplet metastable states, respectively. From $H\ |\psi\rangle = -\frac{\hbar}{i}\frac{\partial}{\partial t}\,|\psi\rangle$, the state amplitudes evolve according to

$$
\begin{aligned}
\dot{c}_{R,k(L,-k)}(t) &= -i\delta_k c_{R,k(L,-k)}(t) + \frac{ig}{\sqrt{2}}(1 + e^{-ikd})c_T(t) \\
&+\frac{ig}{\sqrt{2}}(1 - e^{-ikd})c_S(t), \qquad (3.10)
\end{aligned}
$$

where $\delta_k = v_g k - \omega_{eg}$. If $\Omega_1(t) = \Omega_2(t)$ and $kd = 2n\pi$, where n is an integer, Eq. (3.10) can be substituted into the equation of motion for $c_T(t)$

$$
\begin{aligned}
\dot{c}_T(t) &= -\frac{\Gamma'}{2}c_T(t) + i\Omega_1(t)c_{M_T}(t) \\
&+ig\int dk[c_{R,k}(t) + c_{L,-k}(t)], \qquad (3.11)
\end{aligned}
$$

which yields integral-differential equation involving $c_T(t)$. Imposing a reasonable constraint that in the photon storage process, there is no outgoing field at the end, such that $c_{R,k(L,-k)}(\infty) = 0$, one can obtain an implicit expression for the required pulse shape $\Omega_1(t)$ and the following equation relating the population in the state $|M_T\rangle$

$$\frac{d}{dt}\left|c_{M_T}(t)\right|^2 = -v_g^2/(2\pi g^2)\left(\frac{d}{dt}\left|E_T(t)\right|^2 - \frac{\Gamma_{pl} - \Gamma'}{2}\left|E_T(t)\right|^2\right), \tag{3.12}$$

where $E_T(t) = -\sqrt{2\pi} i g c_T(t)/v_g$. With the normalizing condition, $\int_{-\infty}^{\infty} dt \left|E_T(t)\right|^2 = 1/(2v_g)$, and assuming that the incoming field vanishes at $t = \pm\infty$ $[E_T(\pm\infty) = 0]$ [16], Eq. (3.12) can be integrated to yield $\left|c_{M_T}(\pm\infty)\right|^2 = 1 - 1/P$, where $P \equiv \Gamma_{pl}/\Gamma'$ is the effective Purcell factor. Similarly, it can be easily shown that the storage efficiency into $|M_S\rangle$ state is also equal to $1 - 1/P$ if $\Omega_1(t) = -\Omega_2(t)$ and $kd = (2n+1)\pi$. Note that the metal and radiative losses on the qubits are taken into account in the above derivation. Therefore, the entangled states can be stored with a high efficiency only if the Purcell factor is high enough. Furthermore, the two qubits can be separated in a remote sense, such that one can address a lone qubit without affecting another.

3.3 Remark on experimental realization

Once the entangled state is prepared, how can one verify it? One possible procedure is to inject plasmons from one end and measuring the output signals. For example, if the entangled state $|s_1, g_2\rangle + |g_1, s_2\rangle$ is created, we then inject a plasmon from the left-side. As the plasmon arrives dot-1, pumping it with a energy-selected laser pulse, which only excites dot-1 from "g_1" state to "e_1" state (but can not excite it from "s_1" to "e_1"). The state now becomes $|s_1, g_2\rangle + |e_1, s_2\rangle$. Put two detectors at both ends of the wire. If we get a signal from the right-end, we know that the wave-function collapses into $|e_1, s_2\rangle$ (note that the injected plasmon connects the states "e" and "g"). Driving the state goes back to $|g_1, s_2\rangle$ with an appropriate pulse. Then, injecting a surface plasmon again, but with a pulse on dot-2. This time the surface plasmon will be scattered by $|g_1, s_2\rangle$ since dot-1 is in "g" state and one observes a signal at the left-end. However, if one observes a signal from the left-end initially, we know that the state collapses into $|s_1, g_2\rangle$. When the last pulse is shined on dot-2, the state becomes $|s_1, e_2\rangle$. This time the second plasmon will pass through the two dots without reflection, and one observes a signal at the right-end. As for the non-entangled state, for example: $|s_1, s_2\rangle/|g_1, g_2\rangle$ state, the above procedure gives two transmitted/reflected photons at at the right/left end.

3.4 Conclusion

In summary, we have examined the scattering properties of the surface plasmons in a metal nanowire coupled with two QDs. Not only the metal loss, but also the super-radiant effect is found to influence the reflection properties. A scheme to create remote entangled state is proposed in the presence of metal and radiative losses. We discover that there are two different cases that the maximal entanglement can be achieved. One is when kd is multiple of π, and the other one is when kd and δ satisfy the condition Eq. (3.7). Furthermore, the proposal can also be applied to other physical system. For example, one can easily extend this to the transmission lines (photons) coupled with Cooper pair boxes (qubits). The Hamiltonian is identical to that in Eq. (3.1) [45]. We therefore believe that it could be tested with current technologies.

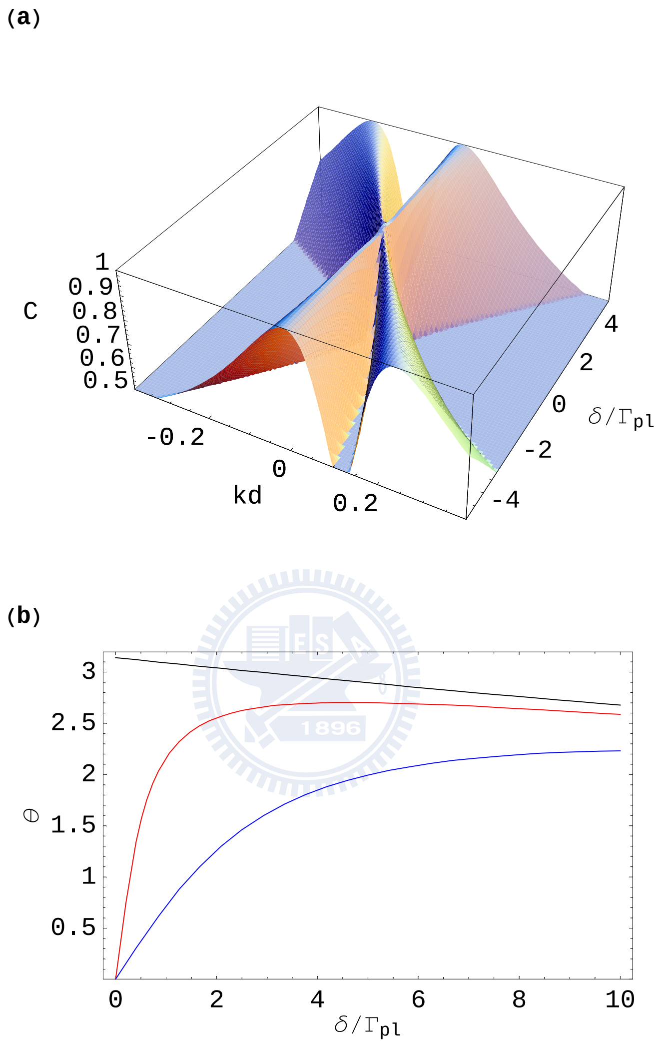

Figure 3.3: (a) Concurrence C of the two-dot qubits as functions of inter-dot distance and detuning δ. (b) The phase factor θ of the entangled state $e_{k_1}|e_1, g_2\rangle + e^{i\theta} \cdot e_{k_2}|g_1, e_2\rangle$ in the limit of $\gamma_0 \to 0$. Black, red, and blue lines represent the results of $\Gamma_0 = 0$, 0.025, and $0.125\Gamma_{pl}$, respectively.

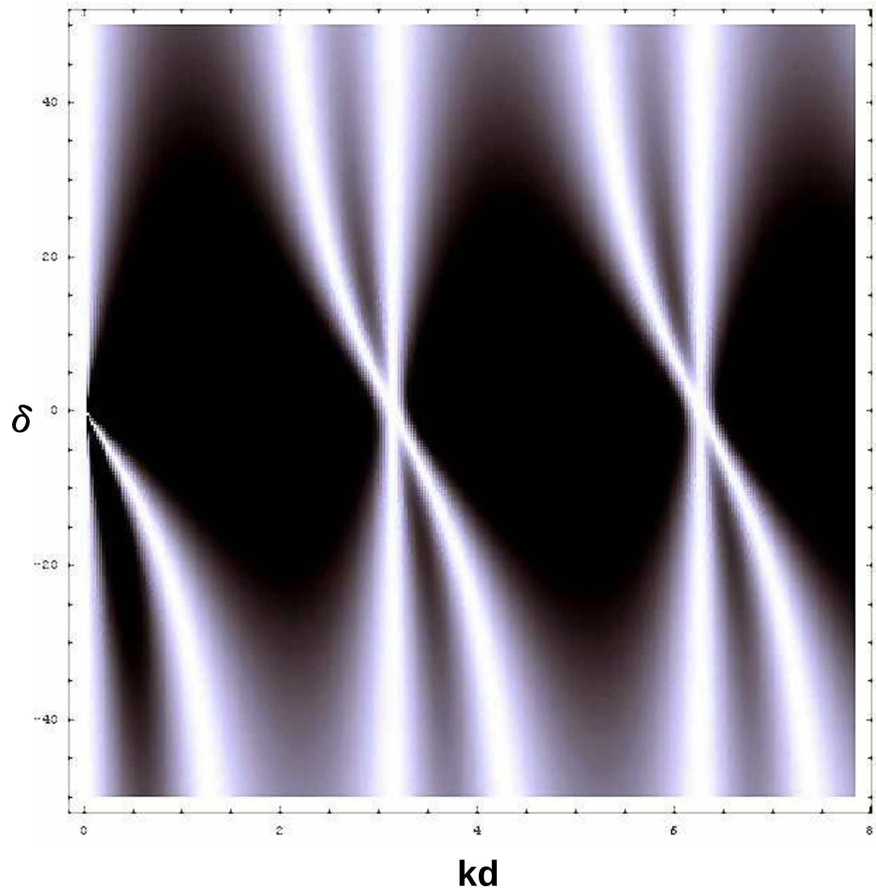

Figure 3.4: The density plot of the concurrence

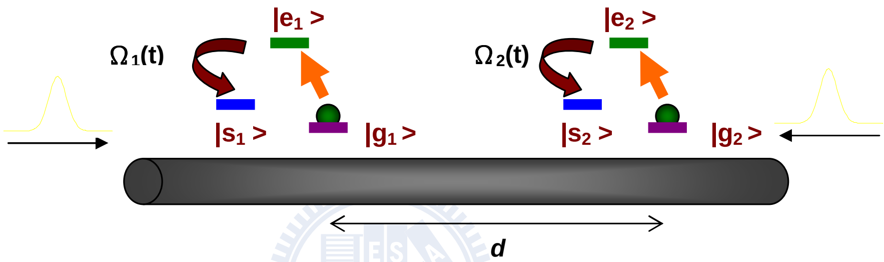

Figure 3.5: Schematic diagram of the storage process into metastable entangled states, $|s_1, g_2\rangle \pm |g_1, s_2\rangle$, with classical optical pulses $\Omega_1(t)$ and $\Omega_2(t)$. To avoid the possible losses in metal nano-wire, a dielectric waveguide is introduced to achieve remote entanglement.

Chapter 4

Entanglement dynamics

The surface plasmons inevitably experience losses as they propagate along the nanowire. It could limit the feasibility in creating remote entanglement. To avoid this, instead of using a infinite long silver nanowire, we consider in this chapter two separate wires with finite length (in the order of 10 nm) evanescently coupled to a phase-matched dielectric waveguide [23]. We also assume the two QDs are coupled to these two wires as shown in Fig. 4.1. In this case, one can have both the advantages of strong coupling from the surface plasmons and long-distance transport by the dielectric waveguide.

By using density matrix treatment and Lindblad form master equations, we will investigate the dynamics of the QD excitons and the corresponding entanglement in this chapter.

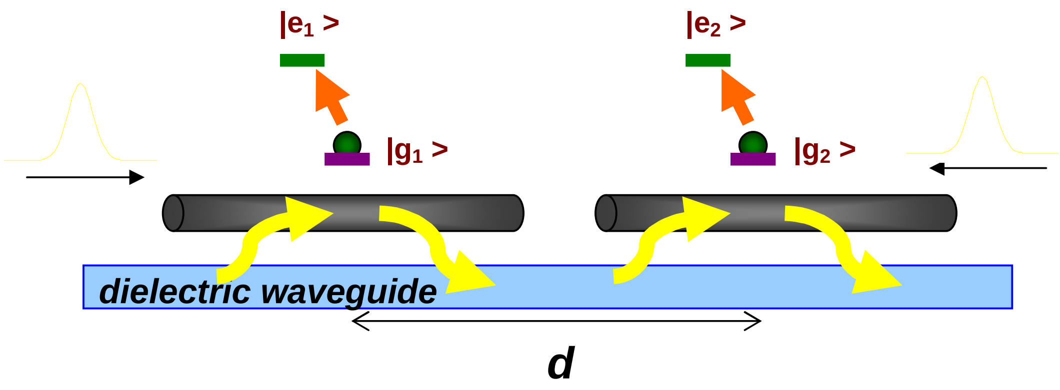

Figure 4.1: Schematic diagram of the two quantum dots coupled to two separate wires with finite length.

4.1 Open quantum system

Let us assume a system S in a superposition of its two basis states, and a second system S' is in a initial state $|\phi_0\rangle$. If there is no interactions (i.e. no correlations) between S and S', the composite state can be written as $|\Psi\rangle = (\alpha\,|A\rangle + \beta\,|B\rangle) \otimes |\phi_0\rangle$, where$|\alpha|^2 + |\beta|^2 = 1$. If we represent this separable state as a density matrix $\rho_{\mathtt{SS'}} = |\Psi\rangle\langle\Psi|$, and trace out the second system S' (i.e. $\rho_{\mathtt{S}} = Tr_{\mathtt{S'}}\rho_{\mathtt{SS'}} = \langle\phi_0\,|\Psi\rangle\langle\Psi|\,\phi_0\rangle$), we obtain a pure state reduced density matrix of system S

$$\sigma_{\mathtt{S}} = \begin{pmatrix} |\alpha|^2 & \alpha\beta^* \\ \alpha^*\beta & |\beta|^2 \end{pmatrix}.$$

But if the system S interacts with the second system S', we say that now the system S is "open", which causes the evolution of S'. Therefore, the state of $\texttt{S}$' would no longer be in $|\phi_0\rangle$ and the composite state is not separable anymore. We can thus write the interacting composite state as $|\Psi\rangle = \alpha |A\rangle |\phi_1\rangle + \beta |B\rangle |\phi_2\rangle$. After tracing out the second system $\texttt{S}$', we again obtain the reduced density matrix $\sigma_{\texttt{S}}$,

$$\rho_{\texttt{S}} = \begin{pmatrix} |\alpha|^2 & \alpha\beta^* \langle\phi_2|\phi_1\rangle \\ \alpha^*\beta \langle\phi_1|\phi_2\rangle & |\beta|^2 \end{pmatrix}.$$

The off-diagonal elements (coherence) is smaller than those in non-interacting case since $\langle\phi_2|\phi_1\rangle < \langle\phi_0|\phi_0\rangle = 1$. This means that the coherence is decreased due to the interactions between systems $\texttt{S}$ and $\texttt{S}$', and the state goes from pure to mixed. In other words, some information of the total system is stored in the entanglement between $\texttt{S}$ and $\texttt{S}$' resulting from the coupling [46].

In the third section of this chapter, we will treat the surface plasmon modes as the second system $\texttt{S}$', and the two QDs as the system $\texttt{S}$. From previous discussions, one realizes that the coherence will be decreased due to the QD-plasmon interactions, and the reduced density matrix will become mixed. To investigate the evolution of the reduced density matrix, in the next section, we will introduce the Lindblad form master equation approach, which is widely used to study time-dependent behaviors.

4.2 Lindblad form master equation

Surface plasmons, propagating electromagnetic waves on the surface of metal nanowires in our model, must be damped due to Ohmic losses or the leakages during transmission (see Fig. 4.1). For two QDs, if they are initially in the ground state, each of them is possible to be excited by the surface plasmons. But meanwhile, they are coupled to the vacuum as well. Therefore, besides decaying into surface plasmons modes, they may also decay into the free space. Since now we consider small nanowires with finite length, the Ohmic losses could be minimized. And, from our previous discussions in chapter 2, the pheonmenon of large Purcell factors due to the strong coupling between dots and surface plasmons should still hold. Thus, we can take these two decay channels : field dampings and spontaneous emissions into free space, as dissipations in our model. Instead of using the quantum jump effective Hamiltonian, we introduce in this section the Lindblad form master equation approach [47], in which the two dissipations are both included.

We start out with a general Hamiltonian, $H = H_{\mathtt{S}} + H_{\mathtt{R}} + H_{\mathtt{SR}}$, where $H_{\mathtt{S}}$ and $H_{\mathtt{R}}$ are Hamiltonian for S and R respectively, $H_{\mathtt{SR}}$ is the interaction between system S and reservoir R. The density matrix corresponding to the total system $\mathtt{S} \oplus \mathtt{R}$ reads $\rho_{\mathtt{SR}} = \rho_{\mathtt{S}} \otimes \rho_{\mathtt{R}}$, while the reduced density matrix of the system is written as $\rho_{\mathtt{S}} = Tr_{\mathtt{R}}\rho_{\mathtt{SR}}$.

The Schrödinger equation of $\rho_{\mathtt{SR}}$ is

$$\dot{\rho}_{\mathtt{SR}} = \frac{1}{i\hbar}[H, \rho_{\mathtt{SR}}], \tag{4.1}$$

we can transform this Schrödinger equation into the interaction picture and get

$$\dot{\tilde{\rho}}_{\mathtt{SR}} = \frac{1}{i\hbar}[\tilde{H}_{\mathtt{SR}}(t), \tilde{\rho}_{\mathtt{SR}}], \tag{4.2}$$

with $\tilde{\rho}_{\mathtt{SR}} = e^{i/\hbar(H_{\mathtt{S}}+H_{\mathtt{R}})t}\rho_{\mathtt{SR}}(t)e^{-i/\hbar(H_{\mathtt{S}}+H_{\mathtt{R}})t}$, and $\tilde{H}_{\mathtt{SR}}(t) = e^{i/\hbar(H_{\mathtt{S}}+H_{\mathtt{R}})t}H_{\mathtt{SR}}(t)e^{-i/\hbar(H_{\mathtt{S}}+H_{\mathtt{R}})t}$. Setting the starting point of interaction is $t = 0$ and integrating Eq. (4.2), we directly obtain

$$\tilde{\rho}_{\mathtt{SR}}(t) = \tilde{\rho}_{\mathtt{SR}}(0) + \frac{1}{i\hbar}\int_0^t dt'[\tilde{H}_{\mathtt{SR}}(t'), \tilde{\rho}_{\mathtt{SR}}(t')]. \tag{4.3}$$

Substituting this back to Eq. (4.2) for $\tilde{\rho}_{\mathtt{SR}}(t)$ inside the commutator gives

$$\dot{\tilde{\rho}}_{\mathtt{SR}} = \frac{1}{i\hbar}[\tilde{H}_{\mathtt{SR}}(t), \tilde{\rho}_{\mathtt{SR}}(0)] - \frac{1}{\hbar^2}\int_0^t dt'[\tilde{H}_{\mathtt{SR}}(t), [\tilde{H}_{\mathtt{SR}}(t'), \tilde{\rho}_{\mathtt{SR}}(t')]], \tag{4.4}$$

where, $\tilde{\rho}_{\mathtt{SR}}(0) = \rho_{\mathtt{SR}}(0) = \rho_{\mathtt{S}}(0)\rho_{\mathtt{R}}(0)$. Because the system S is what we are interested in, after tracing out R, Eq. (4.4) becomes

$$\dot{\tilde{\rho}}_{\mathtt{S}} = \frac{1}{i\hbar}Tr_{\mathtt{R}}\{[\tilde{H}_{\mathtt{SR}}(t), \tilde{\rho}_{\mathtt{SR}}(0)]\} - \frac{1}{\hbar^2}\int_0^t dt' Tr_{\mathtt{R}}\{[\tilde{H}_{\mathtt{SR}}(t), [\tilde{H}_{\mathtt{SR}}(t'), \tilde{\rho}_{\mathtt{SR}}(t')]]\}. \tag{4.5}$$

Since one could always write $\tilde{H}_{\mathtt{SR}}$ as a sum of products of operators s_i of system S and operators R_i of reservoir R,

$$\tilde{H}_{\mathtt{SR}}(t) = \hbar\sum_i \tilde{s}_i(t)\tilde{R}_i(t), \tag{4.6}$$

we assume that the mean value of the observable $\tilde{R}_i$ in state $\rho_{\mathtt{R}}$ is zero (i.e. $Tr[\rho_{\mathtt{R}}\tilde{R}_i] = 0$). We can then eliminate the leading term $\frac{1}{i\hbar}Tr_{\mathtt{R}}\{[\tilde{H}_{\mathtt{SR}}(t), \tilde{\rho}_{\mathtt{SR}}(0)]\}$ with the cyclic property of trace $Tr[ABC] = Tr[BCA] = Tr[CAB]$. Finally, we have

$$\dot{\tilde{\rho}}_{\mathtt{S}} = -\frac{1}{\hbar^2}\int_0^t dt' Tr_{\mathtt{R}}\{[\tilde{H}_{\mathtt{SR}}(t), [\tilde{H}_{\mathtt{SR}}(t'), \tilde{\rho}_{\mathtt{SR}}(t')]]\}. \tag{4.7}$$

If the interaction between the system and reservoir is very weak and the reservoir is relatively large, one can expect the reservoir is virtually unaffected (stay in initial state) during the interaction. Thus, the density matrix of the total system can be expanded as

$$\tilde{\rho}_{\mathtt{SR}}(t) = \tilde{\rho}_{\mathtt{S}}(t)\tilde{\rho}_{\mathtt{R}}(0) + O(H_{\mathtt{SR}}), \tag{4.8}$$

The Born approximation can be made here to neglect the higher order terms in Eq. (4.7) and give

$$\dot{\tilde{\rho}}_{\mathtt{S}} = -\frac{1}{\hbar^2}\int_0^t dt' Tr_{\mathtt{R}}\{[\tilde{H}_{\mathtt{SR}}(t), [\tilde{H}_{\mathtt{SR}}(t'), \tilde{\rho}_{\mathtt{S}}(t')\tilde{\rho}_{\mathtt{R}}(0)]]\}. \tag{4.9}$$

We can now substitute Eq. (4.6) into Eq. (4.9) and obtain

$$\begin{aligned}\dot{\tilde{\rho}}_{\mathtt{S}} = - & \sum_{i,j}\int_0^t dt'\{[\tilde{s}_i(t)\tilde{s}_j(t')\tilde{\rho}_{\mathtt{S}}(t') - \tilde{s}_j(t')\tilde{\rho}_{\mathtt{S}}(t')\tilde{s}_i(t)]\langle\tilde{R}_i(t)\tilde{R}_j(t')\rangle_{\mathtt{R}} \\ + & [\tilde{\rho}_{\mathtt{S}}(t')\tilde{s}_j(t')\tilde{s}_i(t) - \tilde{s}_i(t)\tilde{\rho}_{\mathtt{S}}(t')\tilde{s}_j(t')]\langle\tilde{R}_j(t')\tilde{R}_i(t)\rangle_{\mathtt{R}}\},\end{aligned} \tag{4.10}$$

where,

$$\begin{aligned}\langle\tilde{R}_i(t)\tilde{R}_j(t')\rangle_{\mathtt{R}} &= Tr_{\mathtt{R}}[\tilde{\rho}_{\mathtt{R}}(0)\tilde{R}_i(t)\tilde{R}_j(t')] \\ \langle\tilde{R}_j(t')\tilde{R}_i(t)\rangle_{\mathtt{R}} &= Tr_{\mathtt{R}}[\tilde{\rho}_{\mathtt{R}}(0)\tilde{R}_j(t')\tilde{R}_i(t)].\end{aligned} \tag{4.11}$$

Now, we can use this master equation, i.e. Eq. (4.10), to discuss the two dissipations taking place in our model separately. First, we focus on the field damping dissipation and ignore two QDs for present discussion. Considering the surface plasmon modes as a system, and the modes which damp the surface plasmon fields as a reservoir. The Hamiltonian can be written as

$$\begin{aligned} H_{\mathtt{S}} &= \sum_k \hbar\omega_k a_k^\dagger a_k, \\ H_{\mathtt{R}} &= \sum_j \hbar\omega'_j b_j^\dagger b_j, \\ H_{\mathtt{SR}} &= \sum_{k,j} \hbar(\kappa_{j,k}^* a_k b_j^\dagger + \kappa_{j,k} a_k^\dagger b_j), \end{aligned} \tag{4.12}$$

where ω_k is the energy of the surface plasmons, $a_k^\dagger(a_k)$ denotes the creation (annihilation) operators for each k mode; $b_j^\dagger$ and b_j represent the modes of reservoir with frequencies ω'_j; $\kappa_{j,k}$ denotes the coupling constant between the surface plasmons and reservoir. In our model, these j modes play the role of transmission losses from Ohmic losses and the leakages between dielectric waveguide and nanowires. From Eqs. (4.6) and (4.12), we can specify $\tilde{s}_i$ and $\tilde{R}_i$ respectively as

$$\begin{aligned} \tilde{s}_1 &= \sum_k a_k e^{-i\omega_k t}, \\ \tilde{s}_2 &= \sum_k a_k^\dagger e^{i\omega_k t}, \\ \tilde{R}_1 &= \tilde{R}^\dagger = \sum_j \kappa_{j,k}^* b_j^\dagger e^{i\omega'_j t}, \\ \tilde{R}_2 &= \tilde{R} = \sum_j \kappa_{j,k} b_j e^{-i\omega'_j t}. \end{aligned} \tag{4.13}$$

Substitute Eq. (4.13) into Eq. (4.10), we obtain

$$\begin{aligned}\dot{\tilde{\rho}}_{\mathtt{S}} = - \quad & \sum_k \int_0^t dt' \{ [a_k a_k \tilde{\rho}_{\mathtt{S}}(t') - a_k \tilde{\rho}_{\mathtt{S}}(t') a_k] e^{-i\omega_k (t+t')} \langle \tilde{R}^\dagger(t) \tilde{R}^\dagger(t') \rangle_{\mathtt{R}} + h.c. \\ + \quad & [a_k^\dagger a_k^\dagger \tilde{\rho}_{\mathtt{S}}(t') - a_k^\dagger \tilde{\rho}_{\mathtt{S}}(t') a_k^\dagger] e^{i\omega_k (t+t')} \langle \tilde{R}(t) \tilde{R}(t') \rangle_{\mathtt{R}} + h.c. \\ + \quad & [a_k a_k^\dagger \tilde{\rho}_{\mathtt{S}}(t') - a_k^\dagger \tilde{\rho}_{\mathtt{S}}(t') a_k] e^{-i\omega_k (t-t')} \langle \tilde{R}^\dagger(t) \tilde{R}(t') \rangle_{\mathtt{R}} + h.c. \\ + \quad & [a_k^\dagger a_k \tilde{\rho}_{\mathtt{S}}(t') - a_k \tilde{\rho}_{\mathtt{S}}(t') a_k^\dagger] e^{i\omega_k (t-t')} \langle \tilde{R}(t) \tilde{R}^\dagger(t') \rangle_{\mathtt{R}} + h.c. \}, \qquad (4.14)\end{aligned}$$

where we take the reservoir S to be a thermal equilibrium mixture of states, $\tilde{\rho}_{\mathtt{R}} = \prod_j e^{-\hbar\omega'_j b_j^\dagger b_j / k_B T}(1 - e^{-\hbar\omega'_j / k_B T})$. Then, we can easily have

$$\begin{aligned}\langle \tilde{R}^\dagger(t) \tilde{R}^\dagger(t') \rangle_{\mathtt{R}} &= 0 \\ \langle \tilde{R}(t) \tilde{R}(t') \rangle_{\mathtt{R}} &= 0 \\ \langle \tilde{R}^\dagger(t) \tilde{R}(t') \rangle_{\mathtt{R}} &= \sum_j |\kappa_{j,k}|^2 e^{i\omega'_j (t-t')} \overline{n}(\omega'_j, T), \\ \langle \tilde{R}(t) \tilde{R}^\dagger(t') \rangle_{\mathtt{R}} &= \sum_j |\kappa_{j,k}|^2 e^{-i\omega'_j (t-t')} [\overline{n}(\omega'_j, T) + 1], \qquad (4.15)\end{aligned}$$

with $\overline{n}(\omega'_j, T) = Tr_{\mathtt{R}}(\tilde{\rho}_{\mathtt{R}} b_j^\dagger b_j) = \frac{e^{-\hbar\omega'_j / k_B T}}{1 - e^{-\hbar\omega'_j / k_B T}}$, is the mean photo number for a oscillator with frequency ω_j at temperature T. Here, k_B is the Boltzmann's constant. We can make a change of variable $\tau \equiv t - t'$, Eq. (4.14) then becomes

$$\begin{aligned}\dot{\tilde{\rho}}_{\mathtt{S}} = - \quad & \sum_k \int_0^t d\tau \{ [a_k a_k^\dagger \tilde{\rho}_{\mathtt{S}}(t-\tau) - a_k^\dagger \tilde{\rho}_{\mathtt{S}}(t-\tau) a_k] e^{-i\omega_k (\tau)} \langle \tilde{R}^\dagger(t) \tilde{R}(t-\tau) \rangle_{\mathtt{R}} + h.c. \\ + \quad & [a_k^\dagger a_k \tilde{\rho}_{\mathtt{S}}(t-\tau) - a_k \tilde{\rho}_{\mathtt{S}}(t-\tau) a_k^\dagger] e^{i\omega_k (\tau)} \langle \tilde{R}(t) \tilde{R}^\dagger(t-\tau) \rangle_{\mathtt{R}} + h.c. \}. \qquad (4.16)\end{aligned}$$

For a large reservoir containing infinite modes, we can also change the summation in Eq. (4.15) to an integration by introducing the density of state

$g(\omega)$, that is, $\sum_j \rightarrow \int_0^\infty d\omega' g(\omega')$. The remaining terms of Eq. (4.15) reads

$$
\begin{aligned}
\langle \tilde{R}^\dagger(t)\tilde{R}(t-\tau)\rangle_{\mathtt{R}} &= \int_0^\infty d\omega' e^{i\omega'(\tau)} g(\omega')|\kappa(\omega')|^2 \overline{n}(\omega', T), \\
\langle \tilde{R}(t)\tilde{R}^\dagger(t-\tau)\rangle_{\mathtt{R}} &= \int_0^\infty d\omega' e^{-i\omega'(\tau)} g(\omega')|\kappa(\omega')|^2 [\overline{n}(\omega', T)+1]. \quad (4.17)
\end{aligned}
$$

From Eq. (4.17), we can easily see that if τ is large enough, the oscillating exponential would average other "slow-varying" functions, $g(\omega')$, $\kappa(\omega')$, $\overline{n}(\omega', T)$ to zero, which means, comparing to the evolution time of $\tilde{\rho}_{\mathtt{S}}$, the correlations of reservoir survive only within a very short time scale τ. We can therefore make an approximation to replace $\tilde{\rho}_{\mathtt{S}}(t-\tau)$ by $\tilde{\rho}_{\mathtt{S}}(t)$. This is called Markovian approximation, which states that the evolution of $\tilde{\rho}_{\mathtt{S}}(t)$ depends only on its present state and is independent of its past history. After making this Markovian approximation, Eq. (4.16) turns out to be the master equation in Born-Markovian approximation,

$$
\dot{\tilde{\rho}}_{\mathtt{S}} = \sum_k [\alpha(a_k\tilde{\rho}_{\mathtt{S}}a_k^\dagger - a_k^\dagger a_k \tilde{\rho}_{\mathtt{S}}) + \beta(a_k\tilde{\rho}_{\mathtt{S}}a_k^\dagger + a_k^\dagger\tilde{\rho}_{\mathtt{S}}a_k - a_k^\dagger a_k\tilde{\rho}_{\mathtt{S}} - \tilde{\rho}_{\mathtt{S}}a_k a_k^\dagger) + h.c.] \quad (4.18)
$$

with

$$
\begin{aligned}
\alpha &= \int_0^t d\tau \int_0^\infty d\omega e^{-i(\omega'-\omega_k)\tau} g(\omega')|\kappa(\omega')|^2, \\
\beta &= \int_0^t d\tau \int_0^\infty d\omega e^{-i(\omega'-\omega_k)\tau} g(\omega')|\kappa(\omega')|^2 \overline{n}(\omega', T). \quad (4.19)
\end{aligned}
$$

Since the reservoir correlations, Eq. (4.17), vanish in the limit of large τ, we can therefore extend the τ integration to infinity and obtain

$$\lim_{t\to\infty}\int_0^t d\tau e^{-i(\omega'-\omega_k)\tau} = \pi\delta(\omega'-\omega_k) + i\frac{P}{\omega_k-\omega'}, \tag{4.20}$$

where, P is the Cauchy principal value. α and β are then written as

$$\begin{aligned} \alpha &= \pi g(\omega_k)|\kappa(\omega_k)|^2 + i\Delta_k, \\ \beta &= \pi g(\omega_k)|\kappa(\omega_k)|^2\overline{n}(\omega_k,T) + i\Delta'_k, \end{aligned} \tag{4.21}$$

with

$$\begin{aligned} \Delta &= \int_0^\infty d\omega\frac{g(\omega')|\kappa(\omega')|^2}{\omega_k-\omega'}, \\ \Delta' &= \int_0^\infty d\omega\frac{g(\omega')|\kappa(\omega')|^2}{\omega_k-\omega'}\overline{n}(\omega',T). \end{aligned} \tag{4.22}$$

By substituting $\alpha, \beta, \Delta_k, \Delta'_k$ into Eq. (4.18) and setting $\Gamma_k = 2\pi g(\omega_k)|\kappa(\omega_k)|^2$, and $\overline{n}(\omega',T) = \overline{n}$, we obtain the master equation,

$$\begin{aligned} \dot{\tilde{\rho}}_{\mathsf{S}} &= \sum_k\{-i\Delta_k[a_k^\dagger a_k, \tilde{\rho}_{\mathsf{S}}] + \Gamma_k(a_k\tilde{\rho}_{\mathsf{S}}a_k^\dagger - \frac{1}{2}a_k^\dagger a_k\tilde{\rho}_{\mathsf{S}} - \frac{1}{2}\tilde{\rho}_{\mathsf{S}}a_k^\dagger a_k) \\ &+ \Gamma_k\overline{n}(a_k\tilde{\rho}_{\mathsf{S}}a_k^\dagger + a_k^\dagger\tilde{\rho}_{\mathsf{S}}a_k - a_k^\dagger a_k\tilde{\rho}_{\mathsf{S}} - \tilde{\rho}_{\mathsf{S}}a_k a_k^\dagger)\}. \end{aligned} \tag{4.23}$$

Eq. (4.23) is still in the interaction picture, we can transform it back to Schrödinger picture, and it reads

$$\begin{aligned} \dot{\rho}_{\mathsf{S}} &= \sum_k\{-i(\omega_k+\Delta_k)[a_k^\dagger a_k, \rho_{\mathsf{S}}] + \Gamma_k(a_k\rho_{\mathsf{S}}a_k^\dagger - \frac{1}{2}a_k^\dagger a_k\rho_{\mathsf{S}} - \frac{1}{2}\rho_{\mathsf{S}}a_k^\dagger a_k) \\ &+ \Gamma_k\overline{n}(a_k\rho_{\mathsf{S}}a_k^\dagger + a_k^\dagger\rho_{\mathsf{S}}a_k - a_k^\dagger a_k\rho_{\mathsf{S}} - \rho_{\mathsf{S}}a_k a_k^\dagger)\}. \end{aligned} \tag{4.24}$$

Here, the frequency shift Δ_k is the so-called Lamb shift in quantum electrodynamics, which is generally very small and can be conventionally neglected.

Furthermore, we assume that the total system is at temperature T=0, then the mean photon number $\overline{n}$ is zero. The final master equation in Born-Markovian approximation can be written as

$$\dot{\rho}_{\mathtt{S}} = \frac{1}{i\hbar}[H_{\mathtt{S}}, \rho_{\mathtt{S}}] + \sum_k \Gamma_k (a_k \rho_{\mathtt{S}} a_k^\dagger - \frac{1}{2} a_k^\dagger a_k \rho_{\mathtt{S}} - \frac{1}{2} \rho_{\mathtt{S}} a_k^\dagger a_k). \tag{4.25}$$

Eq. (4.25) is the Lindblad form master equation with Lindblad operator a_k which governs the field damping of the surface plasmons due to Ohmic losses and leakages. Γ_k in Eq. (4.25) is identified as the decay rate of each k mode into this field-damping dissipation channel.

Our next step is to derive the Lindblad form master equation for the dissipation due to the QD excitons decaying into free space. We can now ignore the surface plasmons and start out with the Hamiltonian which describes the interaction between the two dots and vacuum,

$$\begin{aligned} H_{\mathtt{S}'} &= \sum_i \hbar \omega_{e_i g_i} \sigma_{e_i, e_i}, \\ H_{\mathtt{R}'} &= \sum_j \hbar \varpi_j r_j^\dagger r_j, \\ H_{\mathtt{S}'\mathtt{R}'} &= \sum_{i,j} \hbar (\eta_{i,j}^* \sigma_{-_i} r_j^\dagger + \eta_{i,j} \sigma_{+_i} r_j). \end{aligned} \tag{4.26}$$

where $\sigma_{e_i,e_i} = |e_i\rangle\langle e_i|$, $\omega_{e_i g_i}$ denotes the energy spacing for i-th QD with i running from 1 to 2. In the Hamiltonian, $H_{\mathtt{R}'}$ describes the vacuum as harmonic oscillators with frequencies ϖ_j for each j mode. And $H_{\mathtt{S}'\mathtt{R}'}$ is the interaction between the two dots and the vacuum, $\sigma_{+i(-i)} = |e_i\rangle\langle g_i|(|g_i\rangle\langle e_i|)$, and $\eta_{i,j}$ is the coupling constant.

The master equation for the reduced density matrix for the dots can now be easily obtained since the calculation is exactly similar to how we derived Eq. (4.25). Thus, we could have it only by replacing a_k and $a_k^\dagger$ by σ_{-_i} and σ_{+_i} respectively

$$\dot{\rho}_{\mathtt{S}'} = \frac{1}{i\hbar}[H_{\mathtt{S}'}, \rho_{\mathtt{S}'}] + \sum_i \gamma_i(\sigma_{-_i}\rho_{\mathtt{S}'}\sigma_{+_i} - \frac{1}{2}\sigma_{+_i}\sigma_{-_i}\rho_{\mathtt{S}'} - \frac{1}{2}\rho_{\mathtt{S}'}\sigma_{+_i}\sigma_{-_i}), \quad (4.27)$$

where γ_i is exactly the decay rate γ_0 for the dot excitons into free space, which can be exactly evaluated as $\gamma_i = \gamma_0 = \frac{1}{4\pi\epsilon_0}\frac{4\omega_{e_ig_i}^3\wp_i^2}{3\hbar c^3}$ with $\wp_i = e\langle g_i|\hat{q}|e_i\rangle$ denoting the dipole moment of the i-th dot.

Eq. (4.27) is the Lindblad form master equation for the reduced density matrix of the two QDs. It describes the dissipation of spontaneous emission into free space resulting from the coupling to vacuum.

Now, we would like to move back to our model Hamiltonian: $H = H_{\mathtt{S}} + H_{\mathtt{S}'} + H_{\mathtt{SS}'} + H_{\mathtt{R}} + H_{\mathtt{R}'} + H_{\mathtt{SR}} + H_{\mathtt{S}'\mathtt{R}'}$, which describes the two QDs couple to multi-mode surface plasmons (see Fig. 4.1), and the two dissipations discussed before. It can be written as a combination of Eqs. (4.12) and

(4.26) plus the do-surface plasmons interaction $H_{\mathtt{SS'}}$, which is

$$\begin{aligned}
H_{\mathtt{S}} &= \sum_k \hbar\omega_k a_k^\dagger a_k, \\
H_{\mathtt{S'}} &= \sum_i \hbar\omega_{e_i g_i}\sigma_{e_i,e_i}, \\
H_{\mathtt{R}} &= \sum_j \hbar\omega_j' b_j^\dagger b_j, \\
H_{\mathtt{R'}} &= \sum_j \hbar\varpi_j r_j^\dagger r_j, \\
H_{\mathtt{SR}} &= \sum_{k,j} \hbar(\kappa_{j,k}^* a_k b_j^\dagger + \kappa_{j,k} a_k^\dagger b_j), \\
H_{\mathtt{S'R'}} &= \sum_{i,j} \hbar(\eta_{i,j}^* \sigma_{-_i} r_j^\dagger + \eta_{i,j}\sigma_{+_i} r_j), \\
H_{\mathtt{SS'}} &= \sum_k \hbar[(g_{1,k}\sigma_{e_1,g_1} a_k + g_{2,k}\sigma_{e_2,g_2} e^{ikd} a_k) + h.c.],
\end{aligned} \tag{4.28}$$

where $g_{1(2),k}$ is the coupling strength between surface plasmon modes and the first (second) QD, and d is the inter-dot distance. The equation of motion for this total system can be written as

$$\dot{\rho} = \frac{1}{i\hbar}[H, \rho], \tag{4.29}$$

we can exactly expand the H and rewrite Eq. (4.29) as

$$\dot{\rho} = \frac{1}{i\hbar}\{[H_{\mathtt{S}} + H_{\mathtt{R}} + H_{\mathtt{SR}}, \rho] + [H_{\mathtt{S'}} + H_{\mathtt{R'}} + H_{\mathtt{S'R'}}, \rho] + [H_{\mathtt{SS'}}, \rho]\}, \tag{4.30}$$

from Eq. (4.30), we identify that the first commutator corresponds to our discussions for deriving Eq. (4.25), and the second commutator corresponds to Eq. (4.27). After tracing out the reservoirs $\mathtt{R}$ and $\mathtt{R'}$, the remaining terms in the commutator is $H_{\mathtt{S}} + H_{\mathtt{S'}} + H_{\mathtt{SS'}}$, and the equation of motion for the reduced density matrix of a composite system $\chi = \mathtt{S} \oplus \mathtt{S}'$ can be easily obtained :

$$
\begin{aligned}
\dot{\rho}_\chi &= \frac{1}{i\hbar}[H_\chi, \rho_\chi] \\
&+ \sum_k \Gamma_k (a_k \rho_\chi a_k^\dagger - \frac{1}{2} a_k^\dagger a_k \rho_\chi - \frac{1}{2} \rho_\chi a_k^\dagger a_k) \\
&+ \sum_{i=1,2} \gamma_i (\sigma_{-_i} \rho_\chi \sigma_{+_i} - \frac{1}{2} \sigma_{+_i} \sigma_{-_i} \rho_\chi - \frac{1}{2} \rho_\chi \sigma_{+_i} \sigma_{-_i}),
\end{aligned}
\tag{4.31}
$$

where $\rho_\chi = Tr_{\mathtt{R},\mathtt{R}'}\rho$, and $H_\chi = H_{\mathtt{S}} + H_{\mathtt{S}'} + H_{\mathtt{SS}'}$.

Eq. (4.31) contains the two QDs, the surface plasmon modes, the interactions between them, and two kinds of dissipations such as field damping and spontaneous emission into free space. It is exactly the Lindblad form master equation we need to calculate the reduced density matrix of the two dots and to investigate the entanglement generation and its dynamics in the next section by tracing out the surface plasmon modes (system $\mathtt{S}'$).

4.3 Evolution of entanglement

In this section, we will use the Lindblad form master equation approach to calculate the dynamics of reduced density matrix for some systems. We first start out with a simplified model to see how the two kinds of dissipations (field damping and spontaneous emission into free space) damp the populations of the two dot states and the surface plasmon states.

Consider the two QDs couple to only one surface plasmon mode k which is incident from the left end of the first small wire. The schematic diagram is the same as Fig. 4.1. The total system now is $\mathtt{S} \oplus \mathtt{S}'$, and the master equation can be written as

$$\begin{aligned}
\dot{\rho} &= \frac{1}{i\hbar}[H, \rho] \\
&+ \Gamma_k(a_k \rho a_k^\dagger - \frac{1}{2} a_k^\dagger a_k \rho - \frac{1}{2}\rho a_k^\dagger a_k) \\
&+ \sum_{i=1,2} \gamma_i(\sigma_{-_i} \rho \sigma_{+_i} - \frac{1}{2}\sigma_{+_i}\sigma_{-_i}\rho - \frac{1}{2}\rho\sigma_{+_i}\sigma_{-_i}),
\end{aligned} \tag{4.32}$$

where $H = H_{\mathtt{S}} + H_{\mathtt{S}'} + H_{\mathtt{SS}'}$ with

$$\begin{aligned}
H_{\mathtt{S}} &= \hbar\omega_k a_k^\dagger a_k, \\
H_{\mathtt{S}'} &= \sum_i \hbar\omega_{e_i g_i}\sigma_{e_i,e_i}, \\
H_{\mathtt{SS}'} &= \hbar[(g_{1,k}\sigma_{e_1,g_1}a_k + g_{2,k}\sigma_{e_2,g_2}e^{ikd}a_k) + h.c.].
\end{aligned} \tag{4.33}$$

Here, all operators and parameters are identical to those we used in previous section. Since there is only one excitation in the system, we expand the density operator of the total system $\mathtt{S} \oplus \mathtt{S}'$ with the basis:

$$\{|g_1, g_2, 1_k\rangle, |g_1, e_2, 0\rangle, |e_1, g_2, 0\rangle, |g_1, g_2, 0\rangle\}.$$

For convenience we label the basis kets as

$$\begin{aligned}|k\rangle &\rightarrow |g_1, g_2, 1_k\rangle,\\ |2\rangle &\rightarrow |g_1, e_2, 0\rangle,\\ |1\rangle &\rightarrow |e_1, g_2, 0\rangle,\\ |0\rangle &\rightarrow |g_1, g_2, 0\rangle.\end{aligned} \tag{4.34}$$

$|e_1, g_2, 0\rangle(|g_1, e_2, 0\rangle)$ denotes the first (second) QD is in the excited state, and the other one is in the ground state; $|g_1, g_2, 1_k\rangle$ denotes the two dots are both in ground state, and the excitation is in the surface plasmon mode k. Since we take the dissipations into account, we have to include the vacuum state $|0\rangle = |g_1, g_2, 0\rangle$ in our basis. Thus, the matrix representation of the density operator of the total system reads

$$\begin{aligned}&\sum_{n,m=k,2,1,0} |n\rangle\langle n|\dot{\rho}|m\rangle\langle m|\\ &= \frac{1}{i\hbar}\sum_{n,m=k,2,1,0} |n\rangle\langle n|[H,\rho]|m\rangle\langle m|\\ &+\Gamma_k \sum_{n,m=k,2,1,0} |n\rangle\langle n|(a_k\rho a_k^\dagger - \frac{1}{2}a_k^\dagger a_k\rho - \frac{1}{2}\rho a_k^\dagger a_k)|m\rangle\langle m|\\ &+\sum_{i=1,2}\gamma_i \sum_{n,m=k,2,1,0} |n\rangle\langle n|(\sigma_{-_i}\rho\sigma_{+_i} - \frac{1}{2}\sigma_{+_i}\sigma_{-_i}\rho - \frac{1}{2}\rho\sigma_{+_i}\sigma_{-_i})|m\rangle\langle m|.\end{aligned} \tag{4.35}$$

Eq. (4.35) can be simplified as

$$\begin{aligned}
(\dot{\rho})_{nm} &= \frac{1}{i\hbar}(H\rho - \rho H)_{n,m} \\
&+ \Gamma_k(a_k\rho a_k^\dagger - \frac{1}{2}a_k^\dagger a_k\rho - \frac{1}{2}\rho a_k^\dagger a_k)_{nm} \\
&+ \sum_{i=1,2}\gamma_i(\sigma_{-i}\rho\sigma_{+i} - \frac{1}{2}\sigma_{+i}\sigma_{-i}\rho - \frac{1}{2}\rho\sigma_{+i}\sigma_{-i})_{nm}. \qquad (4.36)
\end{aligned}$$

Now we can calculate all elements of the matrices on both sides of Eq. (4.36). These matrices can be flatted and rearranged as

$$\begin{pmatrix} \dot{\rho}_{kk}(t) \\ \dot{\rho}_{k2}(t) \\ \vdots \\ \vdots \\ \dot{\rho}_{01}(t) \\ \dot{\rho}_{00}(t) \end{pmatrix}_{16\times 1} = \begin{pmatrix} A \end{pmatrix}_{16\times 16} \begin{pmatrix} \rho_{kk}(t) \\ \rho_{k2}(t) \\ \vdots \\ \vdots \\ \rho_{01}(t) \\ \rho_{00}(t) \end{pmatrix}_{16\times 1}.$$

Thus, the entire problem turns out to be a system of coupled differential equations. All we need is to diagonalize the intermediate matrix A, and obtain its eigenvalues and eigenvectors to do the linear transformation. In this way, we can decouple the coupled differential equations and obtain the solutions $\rho_{nm}(t)(n, m = k, 2, 1, 0)$ with given initial conditions. In the density matrix of the total system $\mathtt{S} \oplus \mathtt{S}'$, the diagonal elements $\rho_{nn}(t)$ are the probabilities in $|n\rangle$ and the off-diagonal elements $\rho_{nm}(t)(n \neq m)$ are the coherences between $|n\rangle$ and $|m\rangle$. Now we set the two dots are both initially in

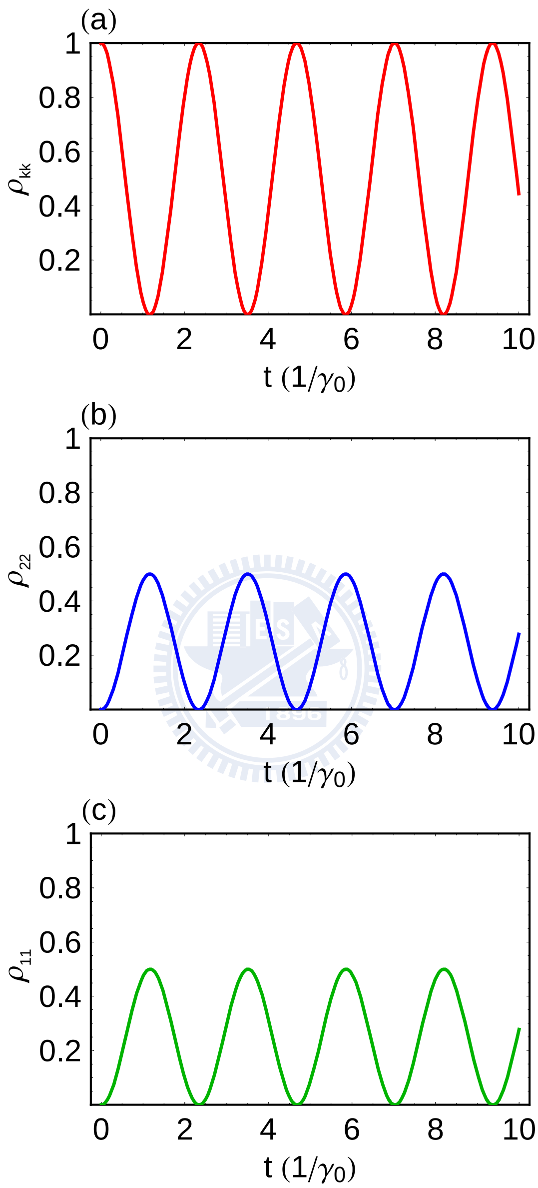

Figure 4.2: Population dynamics without dissipations for each diagonal element.

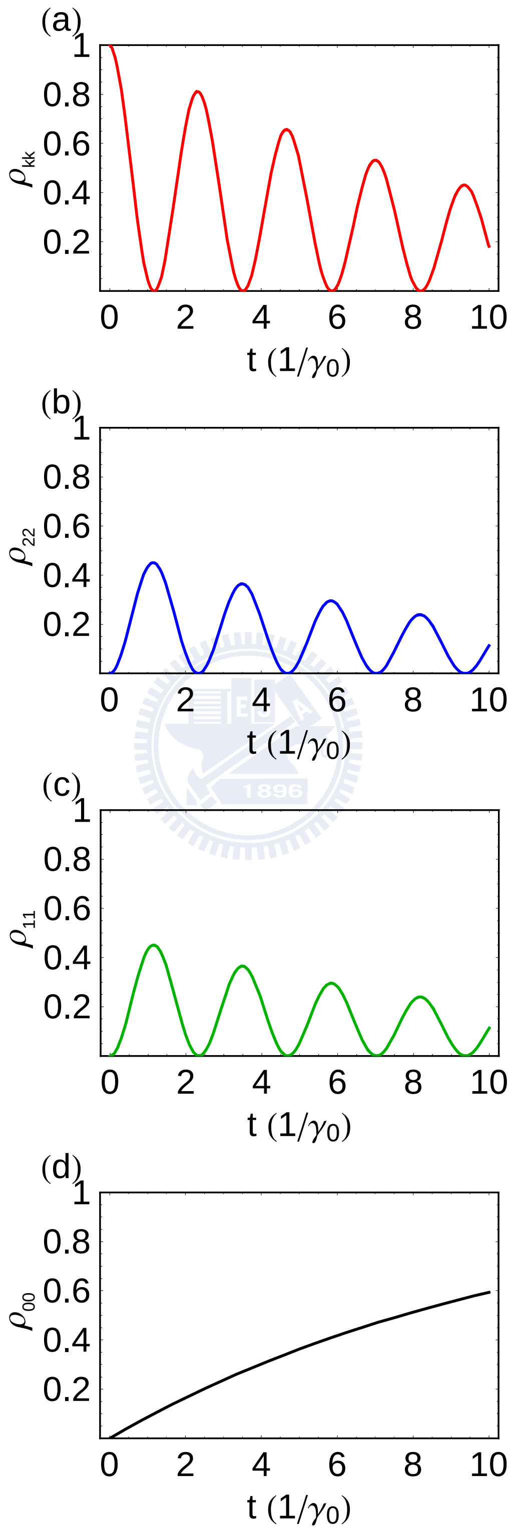

Figure 4.3: Population dynamics with dissipations ($\Gamma_k = \gamma_1 = \gamma_2 = \gamma_0$) for each diagonal element.

the ground state with identical two-level spacing which is resonant with the surface plasmon mode k incident from the left end of the first wire, and the two dissipations have the same decay rate (i.e. $\Gamma_k = \gamma_1 = \gamma_2 = \gamma_0$). In last chapter, we set the Purcell factor $P = 20$, for which the coupling strength between QDs and surface plasmons is about $3\gamma_0$. We further assume that the couplings of the two dots to the surface plasmon mode k are the same. If we first ignore the dissipations (Fig. 4.2), it is similar to that of two identical dots are placed inside a high Q cavity with single mode. Therefore, the populations are independent of inter-dot distance d and reveal the feature of Rabi Oscillations in cavity Q.E.D: going back and forth between the surface plasmon mode k and the two dots [38]. With dissipations, the populations are damped by the two channels individually as shown in Fig. 4.3 (a), (b), (c). Since we assume that the coupling constant g is the same for two dots (i.e. $g_1 = g_2 = g$), panels (b) and (c) of Fig. 4.2 and 4.3 demonstrate that the two dots 'see' the same surface plasmon mode k . Note that in plotting the figure, the unit of time t is normalized to the inverse of free-space decay rate γ_0.

One might argue that it is not sufficient to consider only a single-mode since the QDs are coupled to infinite propagating modes. However, from our discussions in Chapter 2, we realize that the energy spacing of QDs can be tuned such that only the lowest n-mode is effective. In addition, the lengths of the wires considered here are finite. This means the dispersion relations of the surface plasmons are discrete. Therefore, if the QD exciton energy happens to be close to one of the discrete points of the dispersion relations, it is plausible to assume a single-mode model. The difference to the original cavity QED case is that the photon is assumed to be injected from one side of the wire. Thus, one should also take into account the mode $-k$ to denote the reflecting surface plasmon from the other side.

Let us now consider two QDs resonantly coupled to the surface plasmon mode k and its reflecting mode $-k$. The Hamiltonian H can be written as

$$\begin{aligned}
H &= H_{\mathsf{S}} + H_{\mathsf{S'}} + H_{\mathsf{SS'}} \\
H_{\mathsf{S}} &= \sum_{\tilde{k}=k,-k} \hbar\omega_{\tilde{k}} a_{\tilde{k}}^{\dagger} a_{\tilde{k}}, \\
H_{\mathsf{S'}} &= \sum_{i} \hbar\omega_{e_i g_i} \sigma_{e_i,e_i}, \\
H_{\mathsf{SS'}} &= \sum_{\tilde{k}=k,-k} \hbar[(g_{1,\tilde{k}}\sigma_{e_1,g_1} a_{\tilde{k}} + g_{2,\tilde{k}}\sigma_{e_2,g_2} e^{i\tilde{k}d} a_{\tilde{k}}) + h.c.], \qquad (4.37)
\end{aligned}$$

and the corresponding Lindblad form master equation reads,

$$\begin{aligned}
\dot{\rho} &= \frac{1}{i\hbar}[H,\rho] \\
&+ \sum_{\tilde{k}=k,-k} \Gamma_{\tilde{k}}(a_{\tilde{k}}\rho a_{\tilde{k}}^{\dagger} - \frac{1}{2}a_{\tilde{k}}^{\dagger}a_{\tilde{k}}\rho - \frac{1}{2}\rho a_{\tilde{k}}^{\dagger}a_{\tilde{k}}) \\
&+ \sum_{i=1,2} \gamma_i(\sigma_{-_i}\rho\sigma_{+_i} - \frac{1}{2}\sigma_{+_i}\sigma_{-_i}\rho - \frac{1}{2}\rho\sigma_{+_i}\sigma_{-_i}). \qquad (4.38)
\end{aligned}$$

The physical picture is similar to our discussions in Chapter 3: the surface plasmon with wavevector k, is injected from the left end of the first wire. It would be either scattered or absorbed by the two QDs with certain possibilities. If the surface plasmon is trapped between the two dots, it is possible to create the entanglement between this two QDs. We now use the basis

$$\begin{aligned}
|k_-\rangle &\rightarrow |g_1, g_2, 1_{-k}\rangle, \\
|k_+\rangle &\rightarrow |g_1, g_2, 1_k\rangle, \\
|2\rangle &\rightarrow |g_1, e_2, 0\rangle, \\
|1\rangle &\rightarrow |e_1, g_2, 0\rangle, \\
|0\rangle &\rightarrow |g_1, g_2, 0\rangle. \qquad (4.39)
\end{aligned}$$

as a complete set to expand Eq. (4.38), and assuming that, at the initial time $t = 0$, only the state $|g_1, g_2, 1_k\rangle$ is populated. With these, the population dynamics for each basis state can then be calculated.

In Figs. 4.4, 4.5 and 4.6, we show the population dynamics for three different inter-dot distance $kd = \frac{\pi}{2}$, $\frac{\pi}{4}$ and 2π (or π), respectively. Notes that not only the coupling strengths are the same ($g_1 = g_2 = g$), but also the decay rates for dissipations are assumed to be identical. A very interesting point in Fig. 4.4 (a) is that the excitation never goes to the $|g_1, g_2, 1_{-k}\rangle$ state.

Now we can go further to study the entanglement dynamics of the two dots by introducing the "concurrence" [48] as a criterion to quantify the entanglement. For a general state ρ of two qubits, the spin-flipped state is

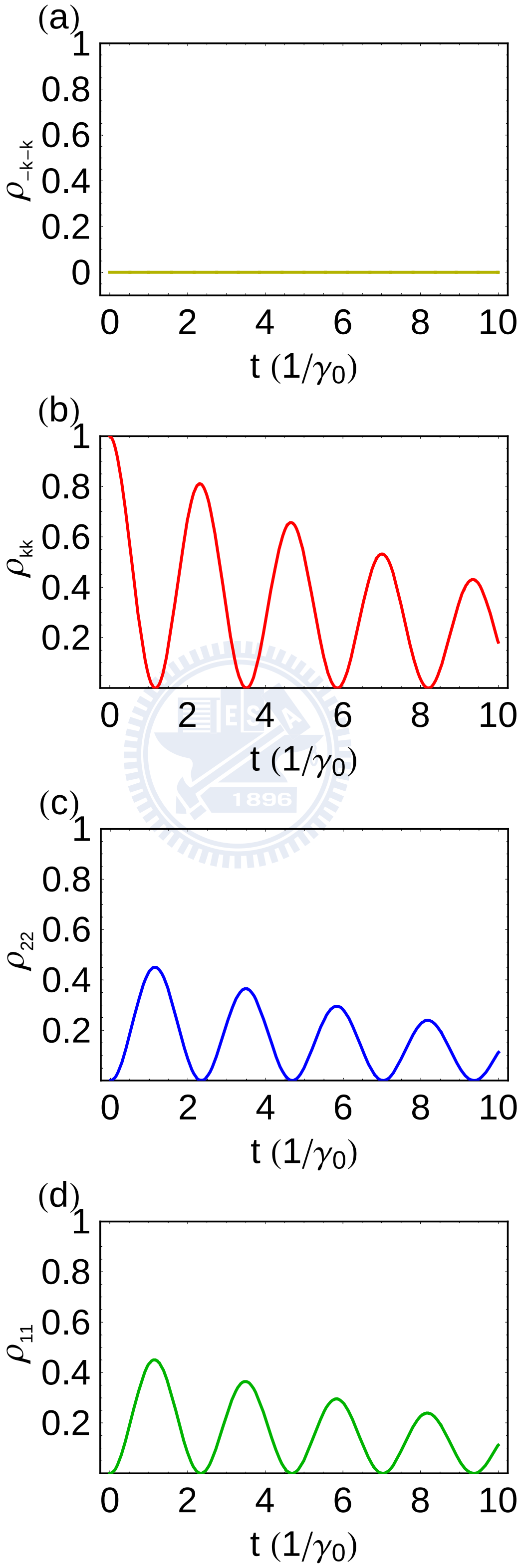

Figure 4.4: Population dynamics with dissipations ($\Gamma_{-k} = \Gamma_k = \gamma_1 = \gamma_2 = \gamma_0$) for $kd = \frac{\pi}{2}$ for each diagonal element.

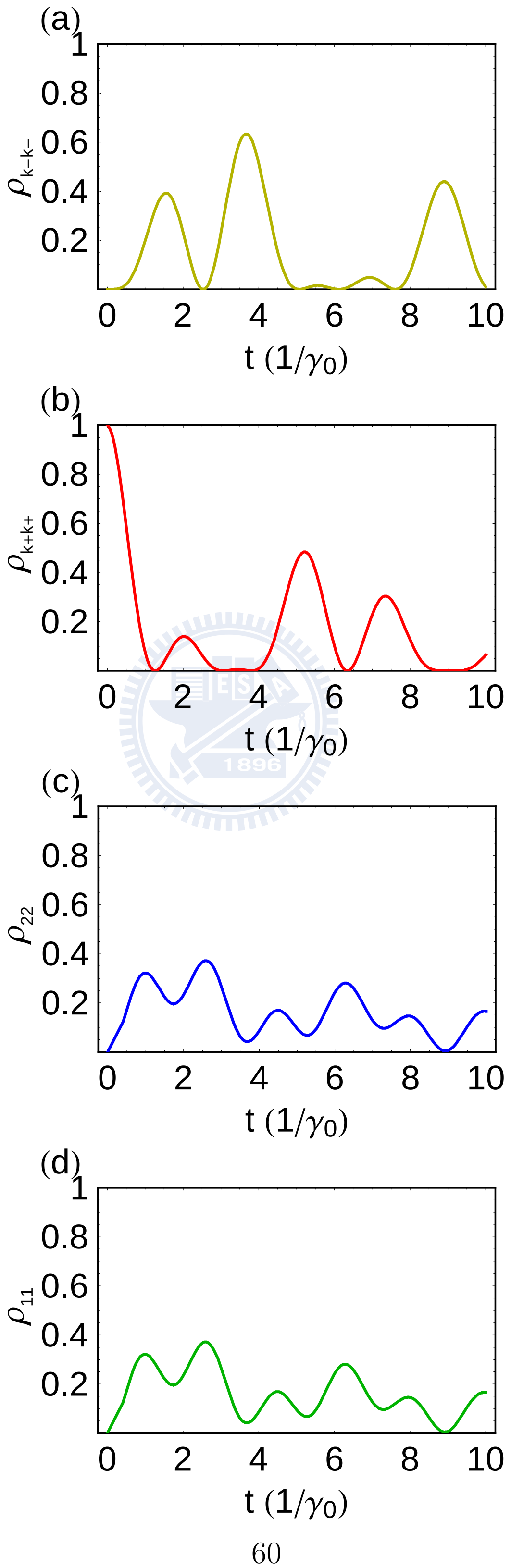

Figure 4.5: Population dynamics with dissipations $((\Gamma_{-k} = \Gamma_k = \gamma_1 = \gamma_2 = \gamma_0))$ for $kd = \frac{\pi}{4}$ for each diagonal element.

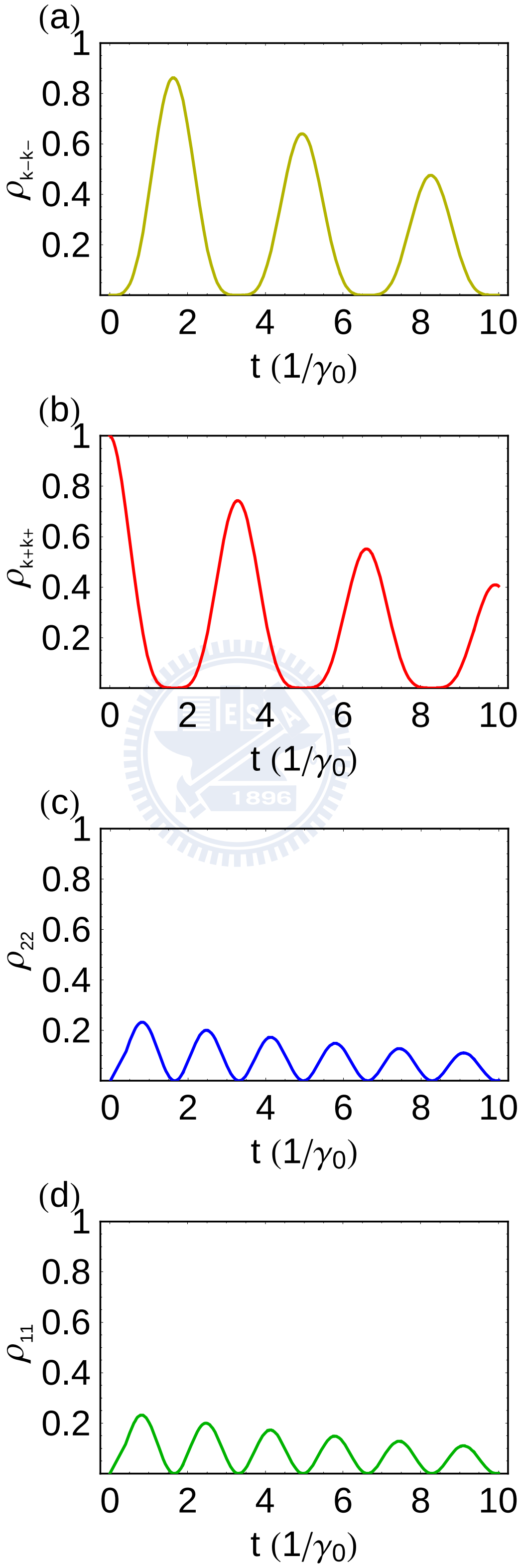

Figure 4.6: Population dynamics with dissipations ($\Gamma_{-k} = \Gamma_k = \gamma_1 = \gamma_2 = \gamma_0$) for $kd = 2\pi$ (or π) for each diagonal element.

written as

$$\rho' = (\sigma_y \otimes \sigma_y)\rho^*(\sigma_y \otimes \sigma_y). \tag{4.40}$$

The concurrence is a positive value between 1 and 0, defined as

$$C(\rho) = max\{0, \sqrt{\lambda_1} - \sqrt{\lambda_2} - \sqrt{\lambda_3} - \sqrt{\lambda_4}\}, \tag{4.41}$$

where σ_y is the y component of Pauli matrices, and $\{\lambda_1, \lambda_2, \lambda_3, \lambda_4\}$ are eigenvalues of $\rho\rho'$ in decreasing order. If all eigenvalues of $\rho\rho'$ are all negative, then the concurrence is zero, which means the state is not entangled at all. For maximally entangled state, the concurrence is unity.

We can therefore use this criterion to quantify the entanglement. First of all, we need to have two qubits, which means we have to trace out the surface plasmons (the system S'):

$$Tr_{\mathtt{S}'}\rho = \langle 1_k|\rho|1_k\rangle + \langle 1_{-k}|\rho|1_{-k}\rangle = \rho_{\mathtt{S}}.$$

Substituting this $\rho_{\mathtt{S}}$ into Eqs. (4.40) and (4.41), we calculate the concurrence for $kd = \frac{(2n+1)\pi}{2}$ $(n = 0, 1, 2...)$, $\frac{(4n+1)\pi}{4}$ $(n = 0, 1, 2...)$, even multiple of π and odd multiple of π for the cases without (with) dissipations shown in Fig. 4.7 (4.8). As see in Fig. 4.7 (a), for $kd = \frac{(2n+1)\pi}{2}$ $(n = 0, 1, 2...)$, we have a periodically maximal entanglement, which is different from our results in Chapter 3. This is because, in Chapter 3, we studied the stationary state which is an average of many measurements. We assume that once there is

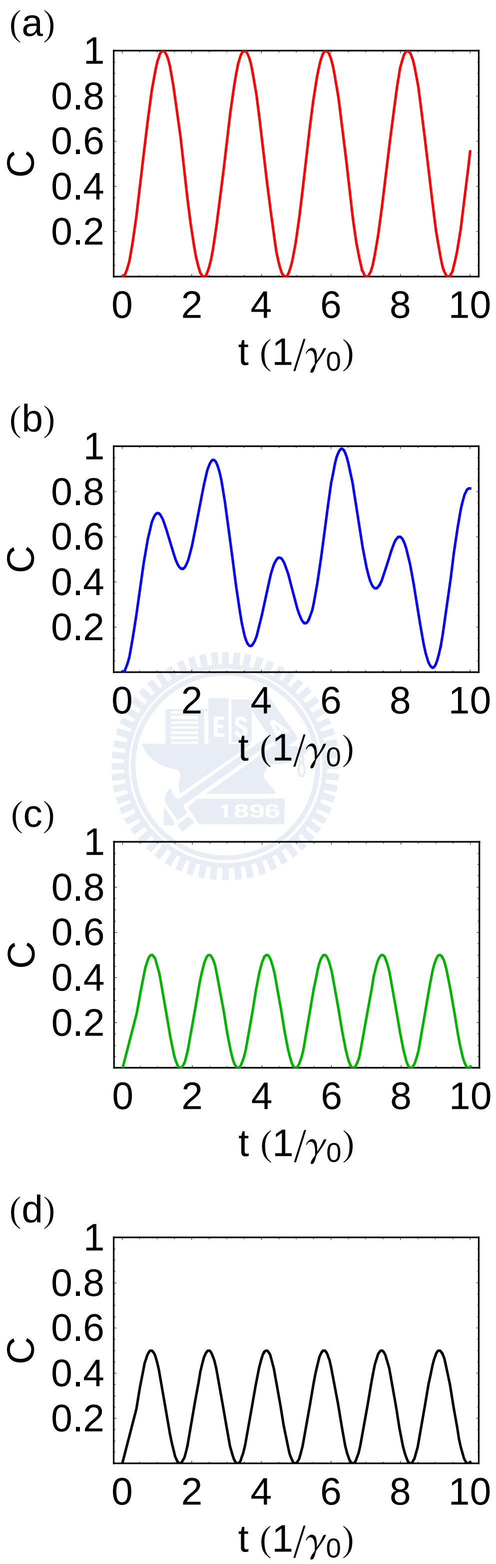

Figure 4.7: The concurrence dynamics without dissipations for kd = (a) $\frac{(2n+1)\pi}{2}$ $(n = 0, 1, 2...)$ (b) $\frac{(4n+1)\pi}{4}$ $(n = 0, 1, 2...)$ (c) even multiple of π and (d) odd multiple of π.

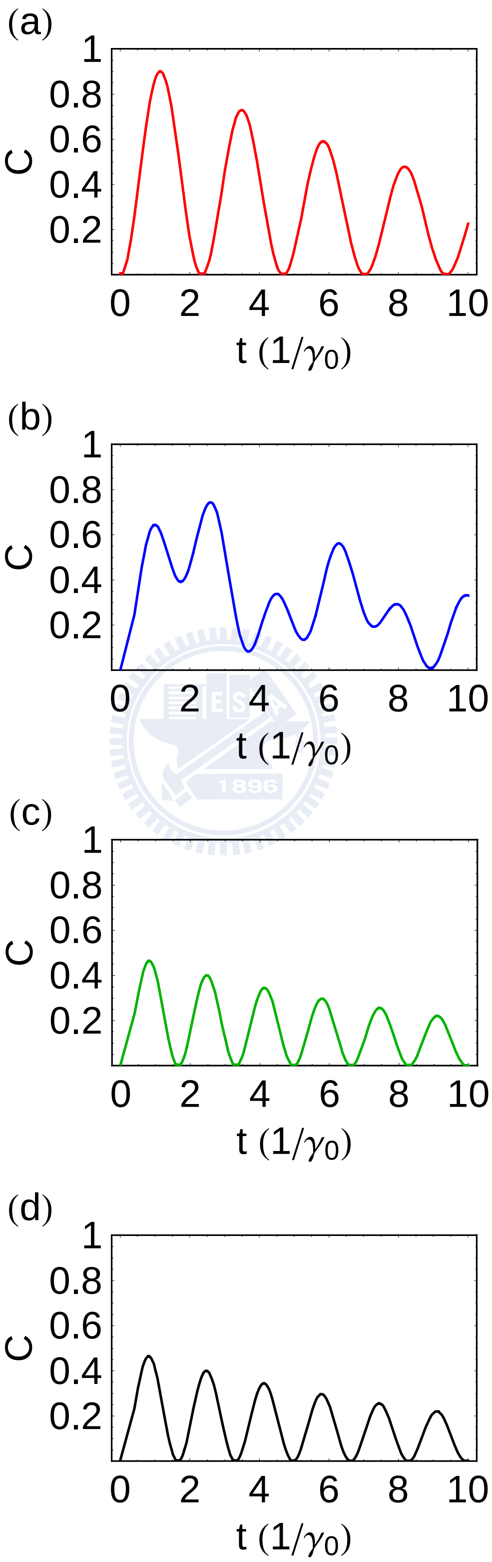

Figure 4.8: The concurrence dynamics with dissipations ($\Gamma_{-k} = \Gamma_k = \gamma_1 = \gamma_2 = \gamma_0$) for $kd =$ (a) $\frac{(2n+1)\pi}{2}$ ($n = 0, 1, 2...$) (b) $\frac{(4n+1)\pi}{4}$ ($n = 0, 1, 2...$) (c) even multiple of π and (d) odd multiple of π.

no detection of any outgoing surface plasmons at the two ends of wire, the total state would be projected into the state of two qubits. Here, however, we include also the probabilities of surface plasmons by using the density matrix ρ. Therefore, for the cases of $kd =$ even multiple of π and odd multiple of π, no maximal entanglement can be created. In addition, since we only take into account two modes here (k and $-k$), some differences are expected if we include more modes. One also notes, in Fig. 4.8, the concurrences decay with time due to dissipations. If one can further reduce the dissipations,higher entanglement can be achieved between the two dots.

In real experiment [15], the samples are prepared by spinning QDs onto a glass substrate with a PMMA layer coverage above. Then, dry silver wires are deposited on top of it. The coupling strength between the QDs and surface plasmons would not be identical for each dot. Therefore, it is desirable to investigate how the concurrence changes with different coupling strengths, i.e. varying $g_{1,\tilde{k}}$ and $g_{2,\tilde{k}}$ in Eq. (4.37). For simplification, we turn off the dissipations and show the concurrences for different coupling strength ratio of the first dot to the second one (Fig. 4.9).

A surprising result is that if g_1/g_2 is a ratio between two odd integers, the concurrence for $kd = \frac{(2n+1)\pi}{2} (n = 0, 1, 2...)$ becomes unity at some points in time. To prove this, we first use Laplace transformation to analytically solve Eq. (4.38). After tracing out the system $\mathtt{S}'$ and obtain the state of the

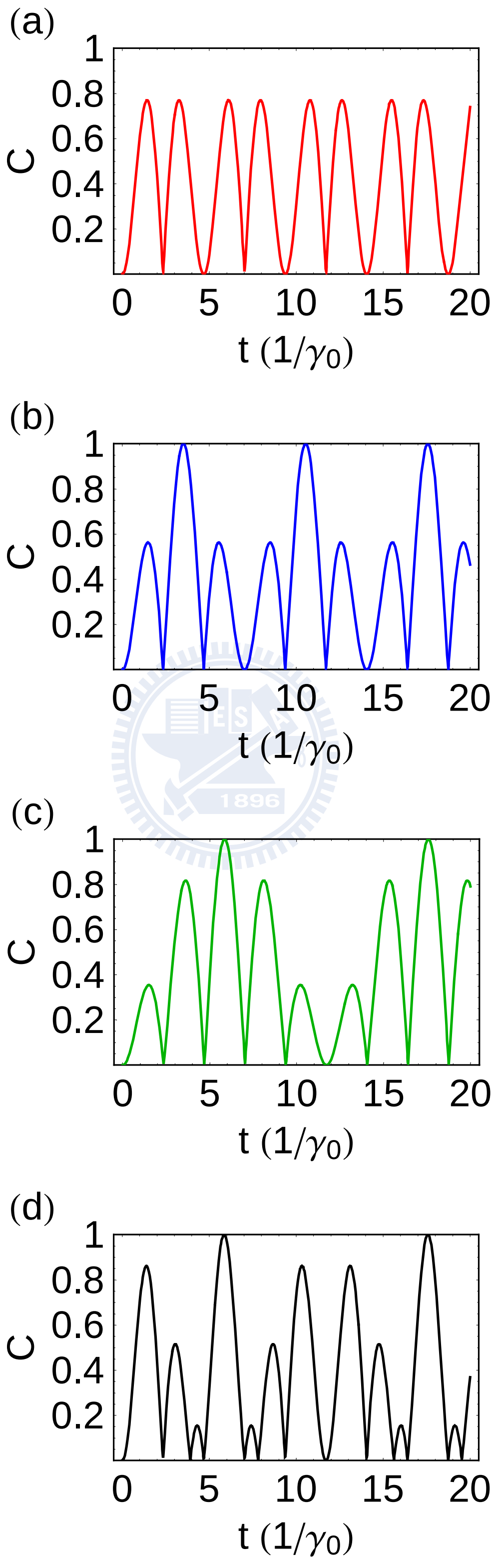

Figure 4.9: The concurrence dynamics for $kd = \frac{(2n+1)\pi}{2}$ $(n = 0, 1, 2...)$ without dissipations for the ratios $g_1/g_2 =$(a) $\frac{1}{2}$ (b) $\frac{1}{3}$ (c) $\frac{1}{5}$ and (d) $\frac{3}{5}$.

two-dot excitons (qubits), we can derive an analytical form of the condition for $C(\rho) = 1$:

$$e^{-i\sqrt{2}(\frac{g_1}{g_2}+1)t}(-1 + e^{2i\sqrt{2}t})(-1 + e^{2i\sqrt{2}\frac{g_1}{g_2}t}) = \pm 4.$$

This equation can be further simplified as

$$Sin(\sqrt{2}\frac{g_1}{g_2}t)Sin(\sqrt{2}t) = \pm 1.$$

One immediately finds that for the requirement of $Sin(\sqrt{2}t) = \pm 1$, the conditions are

$$t = \frac{2\xi + 1}{2\sqrt{2}}\pi \ (\xi = 0, 1, 2, 3...).$$

With the second requirement for $Sin(\sqrt{2}\frac{g_1}{g_2}t) = \pm 1$, one obtains the ratio must satisfy:

$$\frac{g_1}{g_2} = \frac{2\eta + 1}{2\xi + 1} \ (\xi, \eta = 0, 1, 2, 3...), \tag{4.42}$$

to achieve maximum entanglement at some points in time ($t = \frac{2\xi+1}{2\sqrt{2}}\pi$).

Instead of setting the initial state is in $|g_1, g_2, 1_k\rangle$, here, we would like to study two special cases for different initial state. First, we consider that if the state is prepared in a pure state of the two QDs initially:

$$\rho(0) = |\psi(0)\rangle\langle\psi(0)| = \frac{1}{\sqrt{2}}(|e_1, g_2, 0\rangle + |g_1, e_2, 0\rangle)\frac{1}{\sqrt{2}}(\langle e_1, g_2, 0| + \langle g_1, e_2, 0|).$$

We find that, for kd =odd multiple of π, the state will stay in this triplet state without evolving with time, and the concurrence is always unity as shown in Fig. 4.10 (a). This is because the triplet state is a eigenstate of the total Hamiltonian [eq. (4.37)] with eigenvalue $\hbar\omega_{eg}$. So, it is straightforward that an eigenstate will not evolve. But this only holds for two QDs with the same energy spacing $\hbar\omega_{eg}$. Similarly, if the initial state is prepared in the singlet state $\rho(0) = |\psi(0)\rangle\langle\psi(0)| = \frac{1}{\sqrt{2}}(|e_1, g_2, 0\rangle - |g_1, e_2, 0\rangle)\frac{1}{\sqrt{2}}(\langle e_1, g_2, 0| - \langle g_1, e_2, 0|)$, for kd =even multiple of π, the state will not evolve as well with the same reason, and the concurrence is also always unity as shown in Fig. 4.10 (b). Second, if the initial state is prepared in the mixed state $\rho(0) = \frac{1}{2}(|e_1, g_2, 0\rangle\langle e_1, g_2, 0| + |g_1, e_2, 0\rangle\langle g_1, e_2, 0|)$. As shown in Fig. 4.11, the concurrences for different kd are calculated. Surprisingly, for $kd = (2n+1)\frac{\pi}{2}$ ($n = 0, 1, 2...$), the concurrence is always zero. The condition for this is written as

$$\cos^2\left(\frac{1 + e^{ikd}}{e^{i\frac{kd}{2}}}\right) - \cos h^2\left(\frac{1 + e^{ikd}}{e^{i\frac{kd}{2}}}\right) = 0.$$

One can easily simplify it and obtain

$$\frac{1 + e^{ikd}}{e^{i\frac{kd}{2}}} = \pm\, i\ \frac{e^{ikd} - 1}{e^{i\frac{kd}{2}}}.$$

With this, one identifies that when $kd = (2n+1)\frac{\pi}{2}$ ($n = 0, 1, 2...$), the concurrence always vanishes as seen in Fig. 4.11(a).

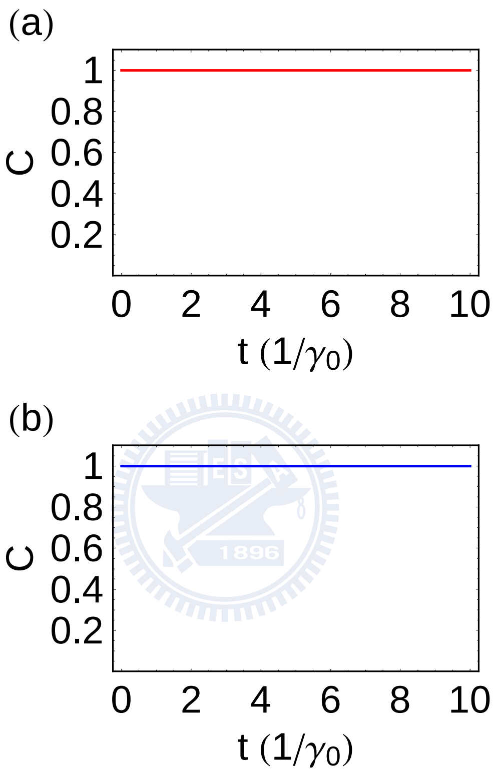

Figure 4.10: The concurrence dynamics for (a) kd=odd multiple of π with $|\psi(0)\rangle$ being the triplet state and (b) kd=even multiple of π with $|\psi(0)\rangle$ being the singlet state.

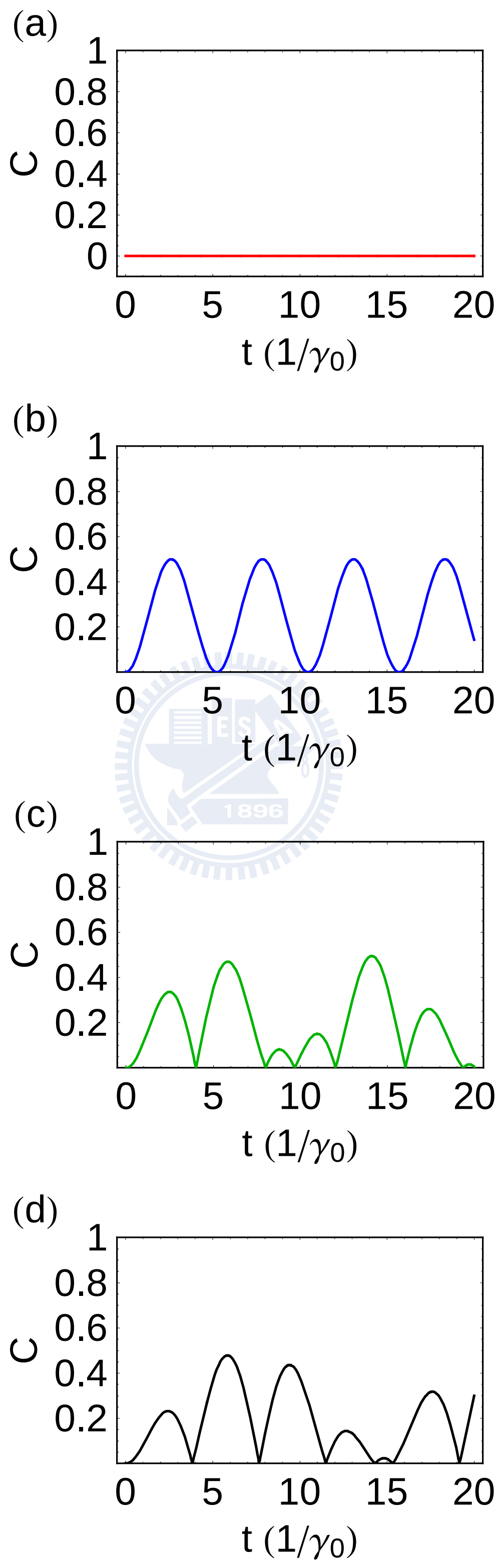

Figure 4.11: The concurrence dynamics without dissipations. The initial state is in the mixed state for $kd =$ (a) $\frac{(2n+1)\pi}{2}$ $(n = 0, 1, 2...)$ (b) multiple of π (c) $\frac{(4n+1)\pi}{4}$ $(n = 0, 1, 2...)$ and (d) $\frac{(3n+1)\pi}{3}$ $(n = 0, 1, 2...)$.

4.4 Conclusion

In this chapter, we keep the main configuration in chapter 3, but alternate the mediator from the infinite long wire to two small wires which are evanescently coupled to the same dielectric waveguide. In this way, one could not only minimize the Ohmic losses resulting from propagating through the metal wire, but also achieve the remote entanglement between the two QDs.

In section 4.1, we introduce the open quantum theory to show how a pure composite density matrix of two systems goes to a mixed reduced density matrix in the presence of interactions between two systems. In the second section, we derive the Lindblad form master equation, which is the main approach we used to study the time dependent behaviors of the system. In the last section of this chapter, we first consider the two QDs coupled to only one resonant surface plasmon mode and apply the master equation to calculate the population dynamics for each basis state. We show that it is legitimate to only take one surface plasmon mode into account because one can tune the energy spacing of the QDs close to the discrete points in the dispersion relations of surface plasmons. We therefore take one surface plasmon mode k which is resonant with the dots plus its reflected mode $-k$ to investigate the entanglement dynamics without dissipations. We find that if the inter-dot distance $kd = \frac{\pi}{2}$, maximal entanglement can be achieved at some points in time when g_1/g_2 equals the ratios of odd integers. We then study two special cases for the initial state prepared in pure and mixed state. It is found that for pure state, the triplet and singlet states don't evolve with time and the maximal entanglement is hold for kd=odd multiple of π and even multiple of π individually. For mixed state, we prove that the concurrence is alwasy zero when $kd = \frac{(2n+1)\pi}{2}$ $(n = 0, 1, 2...)$.

Chapter 5

Summary and outlooks

In this thesis, we make use of the physical properties of surface plasmons to study a series of problems essentially based on the strong interactions between QDs and surface plasmons. In the first chapter, we introduce some backgrounds of the surface plasmons and the motivations. In the second chapter, we apply the Fermi's golden rule to calculate the decay rate of a QD exciton into the surface plasmon modes. We find that the decay rate is greatly enhanced due to the strong coupling between surface plasmon and the QD. The unreasonable infinite enhancement tells us that it is not legitimate to use *Markovian* treatment around the band-edge . We thereby deal with the problem with a *non-Markovian* way, and obtain the oscillatory behaviors of decay dynamics. In the third chapter, we consider a surface plasmon incident from the left end of a long wire to study the scattering resulting from the interactions with two QDs. We find that if there is no out-going surface plasmon detected, the entire state collapses into the entangled state of the two QDs. We also obtain two conditions for achieving maximal entanglement. In the latter part of chapter 3, we propose a way to store the entangled state and a experimental procedure to verify that if the entangled state has been prepared or not. In the last chapter, we keep the main configuration in chapter 3, but use two small wires to replace the original infinite long one to minimize the ohmic losses during propagation. In stead of applying the "projection" concept we used in chapter 3, we use the density matrix approach to obtain the population dynamics of each basis state and introduce the Lindblad form master equation to include the dissipations. After tracing out the surface plasmon modes, we obtain the reduced density matrix of the two QDs, which is used to calculate the concurrence dynamics. We find that when the inter-dot distance $kd = \frac{(2n+1)\pi}{2}$ (n=0,1,2,3...), the maximal entanglement can be achieved. We also investigate that when the ratio of coupling strength of the two QDs equals a ration of two odd integers, the concurrences recover to unity at some points in time for $kd = \frac{\pi}{2}$. In addition, for a triplet (singlet) initial state, the concurrence is always unity for $kd =$ odd (even) multiple of π. For an initially mixed state, we prove that under the condition of $kd = \frac{(2n+1)\pi}{2}$, the concurrence always vanishes. With the advantage of the strong coupling between QDs and surface plasmons, we

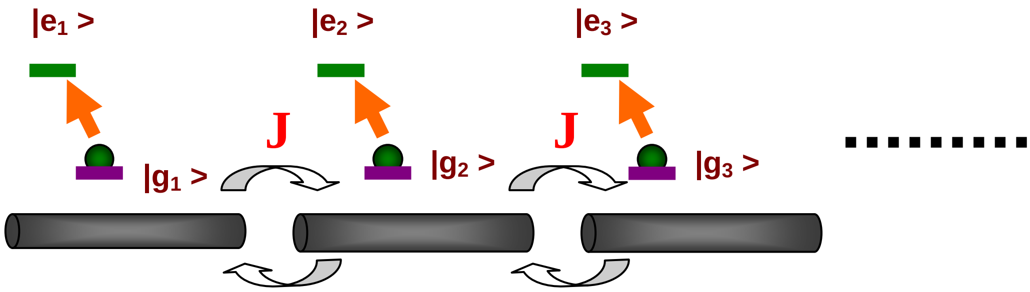

Figure 5.1: The schematic diagram for a one-dimensional array to simulate Bose-Hubbard model.

propose a future work on the simulation of quantum phase transition [27, 28]. Consider a one-dimensional array, each site in this array contains a QD which is put close to a small metal wire (See Fig. 5.1) and is thus coupled to the surface plasmons with coupling strength g. Each site is also coupled to one another with coupling strength J. So, once the surface-plasmonic polariton is created, it can transport back and forth from one site to the next. The Hamiltonian of each cell can be described by a atom-field Hamiltonian plus one hopping term as [27, 49]

$$H = \sum_i H_i^{af} - \sum_{i,j} J_{i,j} a_{k_i}^\dagger a_{k_j} - \sum_i \mu_i N_i, \tag{5.1}$$

with

$$H^{af} = \sum_k \hbar\omega_k a_k^\dagger a_k + \hbar\omega_{eg}\sigma_{ee} + \sum_k \hbar g_k(\sigma_+ a_k + \sigma_- a_k^\dagger). \tag{5.2}$$

Where, H^{af} denotes the atom-field Hamiltonian with g_k denotes the coupling strength between QD and surface plasmon. The second term in Eq. (5.1) is the hopping term with $J_{ij} = J$ denotes the coupling strength for nearest neighbors and $J = 0$ otherwise. $a_{k_i}^{\dagger}$ (a_{k_i}) is the creation (annihilation) operator for $k-$mode surface plasmon at site i, $\sigma_{ee} = |e\rangle\langle e|$ with ω_{eg} is the energy spacing of each dot. ω_k is the frequency of $k-$mode surface plasmon, and $\sigma_{+(-)} = |e\rangle\langle g|$ ($|g\rangle\langle e|$) denotes the atomic creation (annihination) operators; N_i is the total number of photonic and atomic excitations, and μ_i is the chemical potential at site i in the grand canonical ensemble.

In this way, we can regard this system as an analogy [27, 28] to a conventional one-dimensional lattice in condensed matter physics and investigate the Mott insulator-to-superfluid phase transition in our system.

Bibliography

[1] W. Barnes, A. Dereux, and T. Ebbesen, *Nature* **424**, 824 (2003).

[2] R. H. Ritchie, Phys. Rev. **106**, 874 (1957).

[3] C. J. Powell and J. B. Swan, Phys. Rev. **115**, 869 (1959); C. J. Powell and J. B. Swan, Phys. Rev. **116**, 81 (1959).

[4] E. A. Stern and R. A. Ferrell, Phys. Rev. **120**, 130 (1960).

[5] R. Zia and M. L. Brongersma, *Nature Nanotechnology* **2**, 426 (2007).

[6] J. Takahara, S. Yamagishi, H. Taki, A. Morimoto, and T. Kobayashi, Opt. Lett. **22**, 475 (1997).

[7] D. K. Gramotnev, and D. F. P. Pile, Appl. Phys. Lett. **85**, 6323 (2004).

[8] D. F. P. Pile, and D. K. Gramotnev, Opt. Lett. **29**, 1069 (2004).

[9] S. I. Bozhevolnyi, V. S. Volkov, E. Devaux, J. Laluet, and T. W. Ebbesen, *Nature* **440**, 508 (2006).

[10] D. Pacifici, H. J. Lezec, and H. A. Atwater, *Nature Photonics* **1**, 402 (2007).

[11] H. F. Arnoldus and T. F. George, Phys. Rev. A **37**, 761 (1988).

[12] Q. Sun, M. Al-Amri, A. Kamli, and M. S. Zubairy, Phys. Rev. A **77**, 062501 (2008).

[13] A. Neogi, and H. Morkoç, Nanotechnology **15**, 1252 (2004); A. Neogi, H. Morkoç, T. Kuroda, and A. Tackeuchi, Opt. Lett. **30**, 93 (2005).

[14] D. E. Chang, A. S. Sørensen, P. R. Hemmer, and M. D. Lukin, Phys. Rev. Lett. **97**, 053002 (2006); G. Y. Chen, Y. N. Chen, and D. S. Chuu, Opt. Lett. **33**, 2212 (2008).

[15] A. V. Akimov, A. Mukherjee, C. L. Yu, D. E. Chang, A. S. Zibrov, P. R. Hemmer, H. Park, and M. D. Lukin, *Nature* **450**, 402 (2007); Y. Fedutik, V. V. Temnov, O. Schöps, U. Woggon, and M. V. Artemyev, Phys. Rev. Lett. **99**, 136802 (2007).

[16] D. E. Chang, A. S. Sørensen, E. A. Demler, and M. D. Lukin, *Nature Physics* **3**, 807 (2007).

[17] C. H. Bennett and D. P. DiVincenzo, *Nature* **404**, 247 (2000).

[18] T. Pellizzari, S. A. Gardiner, J. I. Cirac, and P. Zoller, Phys. Rev. Lett. 75, 3788 (1995); J. I. Cirac and P. Zoller, Phys. Rev. Lett. **74**, 4091 (1995); K. Molmer and A. Sorensen, Phys. Rev. Lett. **82**, 1835 (1999).

[19] A.T. Costa, Jr. and S. Bose, Phys. Rev. Lett. 87, 277901 (2001); W.D. Oliver, F. Yamaguchi, and Y. Yamamoto, Phys. Rev. Lett. **88**, 037901 (2002); O. Gywat, G. Burkard, and D. Loss, Phys. Rev. B **65**, 205329 (2002).

[20] A. J. Berkley, H. Xu, R. C. Ramos, M. A. Gubrud, F. W. Strauch, P. R. Johnson, J. R. Anderson, A. J. Dragt, C. J. Lobb, F. C. Wellstood, Science **300**, 1548 (2003); M. Steffen, M. Ansmann, R. C. Bialczak, N. Katz, E. Lucero, R. McDermott, M. Neeley, E. M. Weig, A. N. Cleland, J. M. Martinis, Science **313**, 1423 (2006); A. O. Niskanen, K. Harrabi, F. Yoshihara, Y. Nakamura, S. Lloyd, J. S. Tsai, Science **316**, 723 (2007).

[21] J. Majer, J. M. Chow, J. M. Gambetta, Jens Koch, B. R. Johnson, J. A. Schreier, L. Frunzio, D. I. Schuster, A. A. Houck, A. Wallraff, A. Blais, M. H. Devoret, S. M. Girvin, and R. J. Schoelkopf, *Nature* **449**, 443 (2007).

[22] A. L. Pyayt, B. Wiley, Y. Xia, A. Chen, and L. Dalton, *Nature Nanotechnology* **3**, 660 (2008).

[23] B. Dayan, A. S. Parkins, T. Aoki, E. P. Ostby, K. J. Vahala, H. J. Kimble, Science **319**, 1062 (2008).

[24] P. Zijlstra, J. W. M Chon, and M. Gu, *Nature* **459**, 410 (2009).

[25] R. Kolesov, B. Grotz, G. Balasubramanian, R. J. Stohr, A. A. L. Nicolet, P. R. Hemmer, F. Jelezko, and J. Wrachtrup, *Nature Physics* **4**, 470 (2009).

[26] A. Falk, F. H. L. Koppens, C. L. Yu, K. Kang, N. de Leon Snapp, A. V. Akimov, M.-H. Jo, M. D. Lukin and H. Park, *Nature Physics* **5**, 475 (2009).

[27] A. D. Greentree, C. Tahan, J. H. Cole, and L. C. Hollenberg, *Nature Physics* **2**, 856 (2006).

[28] L. Buluta and F. Nori, Sciense **326**, 108 (2009).

[29] I. Gontijo, M. Boroditsky, E. Yablonovitch, S. Keller, U. K. Mishra, and S. P. DenBaars, Phys. Rev. B **60**, 11564 (1999).

[30] G. Schlegel, J. Bohnenberger, I. Potapova, and A. Mews, Phys. Rev. Lett. **88**, 137401 (2002).

[31] C. T. Yuan, W. C. Chou, Y. N. Chen, J. W. Chou, D. S. Chuu, C. A. Lin, J. K. Li, W. H. Chang, and J. L. Shen, J. Phys. Chem. C, **111** (42), 15166 (2007).

[32] J. A. Stratton, *Electromagnetic Theory* (McGraw-Hill, New York, 1941).

[33] C. A.Pfeiffer, E. N. Economou and K. L. Ngai, Phys. Rev. B **10**, 3038 (1974).

[34] P. B. Johnson and R. W. Christy, Phys. Rev. B **6**, 4370 (1972); R. Paiella, Appl. Phys. Lett. **87**, 111104 (2005).

[35] B. H. Hong, S. C. Bae, C. W. Lee, S. Jeong, and K. S. Kim, Science **294**, 348-351 (2001).

[36] From the numerical results, the imaginary parts of ω for the bound modes are actually very small ($10^{-4} \sim 10^{-5}$ of the real parts).

[37] H. T. Dung, L. Knoll, D. G. Welsch, Phys. Rev. A **62**, 053804 (2000). A. A. Asatryan et al, Phys. Rev. E **63**, 046612 (2001). V. Yannopapas and N. V. Vitanov, Phys. Rev. B **75**, 115124 (2007); V. Yannopapas and N. V. Vitanov, J. Phys.: Condens. Matter **19**, 096210 (2007).

[38] Y. Yamamoto and A. İmamoḡlu, *Mesoscopic Quantum Optics* (Wiley, New York, 1999); M. O. Scully and M. S. Zubairy, *Quantum Optics* (Cambridge University Press, Cambridge, 1997).

[39] J. M. Pitarke, V. M. Silkin, E. V. Chulkov, and P. M. Echenique, Rep. Prog. Phys. **70**, 1-87 (2007).

[40] V. Yannopapas, J. Opt. B **6**, 283 (2004).

[41] J. Piilo, S. Maniscalco, K. Harkonen, and K.A. Suominen, Phy. Rev. Lett. **100**, 180402 (2008); S. Maniscalco, S. Olivares, and M. G. A. Paris, Phy. Rev. A **75**, 062119 (2007).

[42] S. John and T. Quang, Phys. Rev. A **50**, 1764 (1994); S. Y. Zhu, Y. Yang, H. Chen, H. Zheng, and M. S. Zubairy, Phys. Rev. Lett. **84**, 2136 (2000); P. Lambropoulos *et al*, Rep. Prog. Phys. **63**, 455 (2000); D. G. Angelakis, P. L. Knight, and E. Paspalakis, Contemp. Phys. **45**, 303 (2004).

[43] D. P. Fussell and M. M. Dignam, Phys. Rev. A **76**, 053801 (2007).

[44] Y. N. Chen, D. S. Chuu, and T. Brandes, Phys. Rev. Lett. **90**, 166802 (2003).

[45] J.-T. Shen and S. Fan, Phys. Rev. Lett. **95**, 213001 (2005); J.-T. Shen and S. Fan, Opt. Lett. **30**, 2001 (2005).

[46] L. Aolita, F. de Melo, and L. Davidovich, private communication.

[47] H. Carmichael, *An Open System Approach to Quantum Optics* (Springer-Verlag, Berlin , 1993); C. Cohen-Tannoudji, J. Dupont-Roc, and G. Grynberg, *Atoms-Photon Interactions : Basic Processes and Applications* (Wiley, New-York, 1992); G. Lindblad, Comm. Math. Phys. **48**, 119V130 (1976).

[48] W. K. Wootters, Phys. Rev. Lett. **80**, 2245 (1998).

[49] L. Zhou, Z. R. Gong, Y. Liu, C. P. Sun, and F. Nori, Phys. Rev. Lett. **101**, 100501 (2008).

Publication list :

1. “Aharonov-Bohm Effect in Concentric Quantum Double Rings”, **Guang-Yin Chen**, Yueh-Nan Chen, and Der-San Chuu, Solid State Communications **143,** 515 (2007).

2. “Proposal for detection of non-Markovian decay via current noise”, Yueh-Nan Chen and **Guang-Yin Chen,** Phys. Rev. B **77**, 035312 (2008).

3. “Spontaneous emission of quantum dot excitons into surface plasmons in a nanowire” , **Guang-Yin Chen**, Yueh-Nan Chen, Der-San Chuu, Opt. Lett. **33**, 2212 (2008)

4. “Quantum-dot exciton dynamics with a surface plasmon: Band-edge quantum optics”, Y. N. Chen, **G. Y. Chen***, D. S. Chuu, and T. Brandes, Phys. Rev. A **79**, 033815 (2009).

5. “Detecting non-Markovian plasmonic band gaps in quantum dots using electron transport”, Yueh-Nan Chen, **Guang-Yin Chen**, Ying-Yen Liao, Neil Lambert and Franco Nori, Phys. Rev. B **79**, 245312 (2009).

6. “Coherent single surface-plasmon transport in a nanowire coupled to double quantum dots”, **G. Y. Chen**, Y. N. Chen, F. Mintert, N. Lambert, D. S. Chuu, and A. Buchleitner, in preparation.